

# The Level of Noise Controls the Efficiency of Natural Selection in Growing Biofilms

Dissertation  
for the award of the degree  
“Doctor rerum naturalium”  
of the Georg–August–Universität Göttingen

within the doctoral program  
International Max Planck Research School  
“Physics of Biological and Complex Systems”  
(IMPRS PBCS)  
of the Göttingen Graduate School for Neurosciences, Biophysics, and  
Molecular Biosciences  
(GGNB)

submitted by  
**Fabian Stiewe**  
from Salzgitter

**Göttingen, 2014**

### **Thesis committee**

**Dr. Oskar Hallatschek**, Biological Physics and Evolutionary Dynamics Group,  
Max Planck Institute for Dynamics and Self-Organization

**Prof. Dr. Christoph F. Schmidt**, Third Institute of Physics, Georg-August-  
Universität Göttingen

**Prof. Dr. Daniel J. Jackson**, Courant Research Centre Geobiology, Georg-  
August-Universität Göttingen

### **Thesis referees**

**Prof. Dr. Christoph F. Schmidt**, Third Institute of Physics, Georg-August-  
Universität Göttingen

**Dr. Eleni Katifori**, Physics of Biological Organization Group, Max Planck Insti-  
tute for Dynamics and Self-Organization

### **Examination committee**

**Dr. Oskar Hallatschek**, Biological Physics and Evolutionary Dynamics Group,  
Max Planck Institute for Dynamics and Self-Organization

**Prof. Dr. Christoph F. Schmidt**, Third Institute of Physics, Georg-August-  
Universität Göttingen

**Prof. Dr. Daniel J. Jackson**, Courant Research Centre Geobiology, Georg-  
August-Universität Göttingen

**Dr. Eleni Katifori**, Physics of Biological Organization Group, Max Planck Insti-  
tute for Dynamics and Self-Organization

**Dr. Iwan Schaap**, Third Institute of Physics, Georg-August-Universität Göttingen

**Prof. Dr. Stephan Herminghaus**, Dynamics of Complex Fluids Group, Max  
Planck Institute for Dynamics and Self-Organization

### **Examination date**

December 11<sup>th</sup>, 2014

I confirm that I have written this thesis independently and with no other sources and aids than quoted.

Goettingen,



# Contents

<b>1. Introduction</b>	<b>9</b>
1.1. Structure of this thesis . . . . .	11
1.2. Range expansions . . . . .	12
1.3. Biofilms . . . . .	12
1.4. Population genetics . . . . .	13
1.4.1. Mutation . . . . .	13
1.4.2. Noise: genetic drift . . . . .	13
1.4.3. Natural selection . . . . .	14
1.5. Sector patterns in microbial colonies . . . . .	15
1.5.1. Formation of sectors . . . . .	15
1.5.2. Difference between species . . . . .	20
1.5.3. Natural selection . . . . .	24
1.6. Aim of this study . . . . .	25
<b>2. Materials and Methods</b>	<b>27</b>
2.1. Microbial strains used in this study . . . . .	28
2.2. Growth media . . . . .	30
2.3. Microscopic imaging and time-lapse movies . . . . .	31
2.4. Testing the influence of cell shape on genetic drift . . . . .	31
2.5. Growth curves . . . . .	32
2.5.1. Liquid culture . . . . .	32
2.5.2. Colonies . . . . .	32
2.5.3. Time-lapse . . . . .	33
2.6. Colony assays . . . . .	33
2.6.1. General procedure . . . . .	33
2.6.2. Systematic assays . . . . .	33
2.7. Determining initial portion of mutant cells . . . . .	35
2.8. Measuring the establishment rate . . . . .	36
2.8.1. Sector numbers and mutant portion . . . . .	36
2.8.2. Estimation of errors in establishment rate $E$ . . . . .	36
2.9. Determining fitness differences . . . . .	37
2.9.1. Estimation of errors in fitness advantage . . . . .	40
2.10. Controls: varying inoculation volume and total cell concentration . . . . .	40

## Contents

<b>3. Results</b>	<b>43</b>
3.1. Influence of cell shape on genetic drift . . . . .	43
3.2. Influence of growth temperature on genetic drift . . . . .	48
3.2.1. Liquid culture . . . . .	48
3.2.2. Colonies . . . . .	51
3.2.3. Time-lapse . . . . .	54
3.3. Sector number is proportional to initial mutant portion . . . . .	56
3.4. Establishment rates for different species and different growth temperatures . . . . .	58
3.5. Control: Influence of inoculation volume . . . . .	65
3.6. Control: Influence of total cell concentration . . . . .	67
<b>4. Discussion</b>	<b>69</b>
4.1. Rod-like cell shape promotes high noise . . . . .	69
4.2. Growth temperature influences noise level . . . . .	70
4.3. Number of establishment events is proportional to mutant portion . . . . .	70
4.4. Establishment rates range over three orders of magnitude . . . . .	70
4.5. Variations of inoculation volume . . . . .	71
4.6. Establishment rate is independent of total cell concentration under crowded conditions . . . . .	71
4.7. Conclusion . . . . .	72
<b>5. Outlook</b>	<b>73</b>
<b>A. Biochemical protocols</b>	<b>75</b>
A.1. Competent <i>E. coli</i> . . . . .	75
A.1.1. Composition of transfer buffer 1 (TFB1) . . . . .	75
A.1.2. Composition of transfer buffer 2 (TFB2) . . . . .	75
A.1.3. Procedure . . . . .	76
A.2. Transformation of <i>E. coli</i> . . . . .	76
A.2.1. Procedure . . . . .	76
<b>B. Microscopy</b>	<b>77</b>
<b>C. Colonies</b>	<b>81</b>
<b>D. Estimation of errors in establishment rate</b>	<b>85</b>
<b>Bibliography</b>	<b>89</b>
<b>CV</b>	<b>95</b>

# Abstract

Many microbes live in biofilms, which are spatially structured populations [1] [2]. During adaptation to a new environment, beneficial mutations occur, and some of them spread through the population. Others go extinct due to noise in the life cycle and reproduction process. This noise is called genetic drift. Growing biofilms are an example of populations undergoing a range expansion. The level of noise in growing biofilms differs strongly between species [3] [4]. However, the effect of these different noise levels on the establishment of beneficial mutations has not yet been quantified. Here we show, that the observed differences in noise level indeed lead to large differences in the establishment rates of beneficial mutations. We found establishment rates of *S. cerevisiae* and spherical *E. coli* strains to be 1–2 orders of magnitude larger than establishment rates of rod-like strains of *E. coli*. Furthermore we observed that the noise level can be tuned via growth temperature, and that the establishment rates measured at different temperatures are consistent with the respective noise levels. Our results suggest that the efficiency of natural selection in biofilms strongly depends on the species and growth conditions. The method presented in this study can be used to test the dependence of establishment rates on other parameters and for many microbial species easily.

*Contents*

# 1. Introduction

Life on earth emerged more than three billion years ago [5] [6] and has generated a plethora of different species [7]; and the evolution of life is still an ongoing process. The genetic composition of populations changes, new species develop and diversify, others go extinct.

In the history of many species, range changes have played an important role [8] [9] [10]. The habitats of these species — the areas they live in — have changed over time, often driven by changes in the environment, for example regarding the climate or food supply. Range changes are also part of the history of humans, that evolved in Africa and eventually spread all over the world's landmass except the polar regions [11] [12]. The type of range changes we look at in this study are continual expansions of the habitat. In terms of evolution, range expansions have dramatic effects on the genetic composition of the population [13].

One way of studying evolution is modeling evolutionary processes theoretically and comparing the results with actual genetic data of existing populations [11]. This way one can gain insights into the history of these populations.

In this study we follow the complementary approach. We investigate evolution experimentally, watching evolution "live at work". Of course, this cannot be done with arbitrary species. Microbes are an excellent system for experimentally studying evolution for several reasons [14].

Microbial populations can be huge (billions of individuals) in a very small habitat (for example a test tube or a petri dish). Also, microbes usually have very short division times — down to less than one hour. Thus, one can watch evolution over many generations in real-time. Additionally, the environment needed for microbes to live and proliferate often is very simple and can be well-controlled and modified. Liquid growth medium or an agar plate in a petri dish containing the necessary nutrients is enough to keep the cells alive and dividing. Altogether this allows for replicate experiments. One can test an evolutionary process with many populations under the same conditions. Replicate experiments are the key feature that allows for quantification and strong statistical statements. Moreover, many microbes can be sequenced and genetically modified with relatively little effort. Hence, one can pointedly test the impact of particular mutations or label strains

## 1. Introduction

for examination. Lastly, microbes can be stored frozen for long time without being killed. Thus, in an evolution experiment one can keep a "frozen time record" of the process and eventually compare microbes from different generations. These properties altogether make microbes a perfect system for the experimental study of evolutionary processes. The most common microbial species used are the bacteria *Escherichia coli* and the baker's yeast *Saccharomyces cerevisiae*. Both of them were also used in this study.

To design experiments and interpret their results, a mathematical framework is needed. The mathematical framework for describing evolutionary processes is population genetics [15]. Population genetics deals with the distribution of genetic variants in a population and its dynamics. Several phenomena are involved in evolution, some of which introduce new genetic variants into a population, some remove genetic variants, and some redistribute them. In this study we focus on the three central processes in evolution and their interplay: mutation, natural selection and genetic drift. We explain these processes in detail in section 1.4. We are particularly interested in the role of genetic drift and the establishment of beneficial mutations in microbial populations.

So far, there are a number of studies on the experimental evolution of microbes. One of the most outstanding is the (still ongoing) long-term evolution experiment conducted by Richard Lenski [16]. Lenski started his experiment in 1988. He founded twelve replicate populations from a single ancestor and introduced them into a new, glucose-limited culture medium. These populations have been propagated via daily transfers to fresh medium, and their evolution has been monitored. In 2010, the populations reached 50,000 generations. One of Lenski's findings was, that the populations adapted quite rapidly to the new environment during the first 2000 generations and then adaptation slowed down, albeit it still continued.

Lenski's long-term evolution experiment surely marks a major progress in experimental evolution of microbes. However, like many other studies investigating microbial evolution [17] [18] [19], Lenski's experiment focusses on well-mixed liquid-culture populations. These populations are isotropic; there is no spatial structure in the microbes' habitat. In nature, many species in fact live in spatially structured habitats, and there are many interesting phenomena that are distinctive of spatially structured habitats. Studies suggest that the dynamics of adaptation are qualitatively different between well-mixed ("zero-dimensional") and spatially explicit habitats [20] [21] [22] [23].

In this study we look at range expansions, a spatially explicit process. By construction, range expansions cannot be studied on the basis of well-mixed populations. Actually, in nature many microbial species form biofilms, which are spatially structured populations and therefore the natural choice for the experimental system

wanted. One example of biofilms in the lab are microbial colonies on a petri dish. A growing colony is a population undergoing a range expansion, so some aspects of range expansions can be studied experimentally in growing colonies.

Hallatschek et al. have introduced a particular type of experiments with microbial colonies [3]. They grew colonies composed of two differently labeled fluorescent strains. When imaging the mature colonies, they observed characteristic sector patterns. A sketch of these sector patterns is shown in Figure 1.1; Figure 1.4 and Figure 1.5 show microscope images of real colonies. The sector patterns render genetic drift visible: in each sector only one of the genetic variants (fluorescence colors) survives.

The colony sector patterns look different for different microbial species. In particular *E. coli* colonies exhibit less sectors than colonies of *S. cerevisiae*. Also the boundaries between the sectors look different – ragged in the case of *E. coli* and straight in the case of *S. cerevisiae*. Hallatschek et al. concluded that the reduction of genetic diversity during the range expansion due to genetic drift is much higher for *E. coli* than for *S. cerevisiae*. This is very different from well-mixed liquid cultures in which genetic drift primarily depends on the population size and not on the species..

In this study we investigate the effect of the differences in genetic drift between species on the efficiency of natural selection. In particular, we test, at which rate beneficial mutations are established in a microbial colony.

## 1.1. Structure of this thesis

The structure of this thesis is as follows. First, we introduce range expansions and show their importance in different types of species. We then provide information about biofilms, which are our model system. Afterwards we introduce some of the concepts of population genetics, in particular mutation, selection and genetic drift. Our focus is on growing microbial colonies on a petri dish. We show that these colonies exhibit particular sectoring patterns. We compare the sectoring patterns generated by different species and present the general aim of this study.

In chapter 2 we list the microbial strains and growth media we used for this study. We present the microscopy techniques used for imaging colonies. We then describe the experiments that we have conducted, the main part of which are competition assays for measuring establishment rates.

In chapter 3 we present our results. First, we shine a light on the connection between noise in sector patterns and biophysical properties of the microbes. We

## 1. Introduction

then show that there is indeed a difference in establishment rate between low-noise and high-noise systems. We also show that inoculation volume and total cell concentration do not have a major impact on these establishment rates.

In chapter 4 we discuss our results and the significance of our study in the framework of evolutionary biology.

In the last chapter we present ideas for further investigations regarding this topic.

## 1.2. Range expansions

A species' habitat is usually not stationary. Instead, it changes over time, for instance due to environmental conditions like climate and food supply [8] [9] [10]. At the end of the last ice age for example, when the temperature increased and the glaciers retreated, many species on the northern hemisphere expanded their habitats northwards [8]. In the history of life on earth many species have undergone such range changes.

In the following we have a look at range expansions in particular, for they exhibit a number of important and interesting phenomena. Consider a large population that colonizes a new territory. Typically only a small fraction of the whole population takes part in the active colonization process. We call this fraction a founder population.

Since it is much smaller than the whole population, the genetic diversity of this founder population typically is also much smaller than the genetic diversity of the original population. All individuals living in the new territory will be descendants of the founder population: their genetic diversity is reduced compared to the starting population, until mutation, recombination and migration bring back the population into equilibrium. Hence, range expansions are accompanied by a genetic bottleneck.

## 1.3. Biofilms

Biofilms are multicellular communities held together by a self-produced extracellular matrix. They grow on all kinds of surfaces: on plants [24], inside pipes [25] and on human teeth [26]. By construction, biofilms have a spatial structure. Overviews on the topic of biofilms can be found for instance in [1] or [2]. Biofilms provide numerous benefits. They can confer resistance to antimicrobial agents and offer protection against host defenses [27]. Biofilms often consist of specialized subpopulations, which differ by gene expression levels. The majority of microbes can form biofilms.

Some examples of well-studied biofilm-forming species are *Escherichia coli* [28], *Bacillus subtilis* [29], *Pseudomonas aeruginosa* [30] [31], *Staphylococcus aureus* [32] and *Saccharomyces cerevisiae* [33]. Since the formation of biofilms is so prevalent among microbial species, in this study we focus on evolutionary dynamics in a particular biofilm, namely microbial colonies on a petri dish.

## 1.4. Population genetics

Population genetics is the mathematical theory that describes the dynamics of the frequencies of genetic variants in a population. An introduction to population genetics can be found for instance in [15]. Population genetics involves a variety of processes: mutation, recombination, horizontal gene transfer, genetic drift and natural selection. This list is possibly far from being complete [34]. In our study we focus on three key processes that we introduce in the following: mutation, genetic drift and natural selection. Mutation increases the genetic diversity of a population, whereas genetic drift and natural selection reduce diversity.

### 1.4.1. Mutation

Mutations are changes of the DNA. These can be substitutions of single base pairs (single nucleotide polymorphisms, SNPs), deletions, insertions or substitutions of extended sequences, up to large rearrangements. If mutations occur within the coding region of the DNA, the encoded protein can change. Even small mutations that only change one amino acid in the protein's polypeptide sequence can have drastic effects. Outside the coding region mutations can affect the expression level of proteins.

In this study we only consider the impact of mutations on the growth and proliferation rate of the microbes. Therefore, we classify mutations with respect to that impact. Mutations that increase the growth rate are called beneficial, ones that decrease the rate are referred to as deleterious. Mutations that do not affect growth rate are called neutral.

### 1.4.2. Noise: genetic drift

Genetic drift refers to the stochasticity in the life cycle and the reproduction process. If individuals die by chance before they can reproduce, they do not contribute to the genetic composition of later generations. Genetic drift plays a major role

## 1. Introduction

in small populations, because in this case death of one individual reduces the relative frequency of its genetic variant in the population significantly. Population bottlenecks — spontaneous drastic reductions of population size — are an important example of situations in which genetic drift becomes crucial. In experiments with microbes this happens for instance in a dilution step. Dilutions steps are necessary to provide new nutrients. For instance, in Lenski’s long-term evolution experiment, every day a sample of the cell culture is diluted in fresh medium; the remains of the old culture are not propagated further. In our experiments there is a ‘continual bottleneck’: only the cells at the very edge of a growing colony contribute to the range expansion. A comparison of Lenski-type experiments and growing biofilms is sketched in Figure 1.3.

### 1.4.3. Natural selection

Selection is the process that changes frequencies of heritable traits that affect the growth and reproduction rate of individuals carrying these traits. If a genetic variant leads to faster proliferation, individuals carrying this variant will increase in frequency. The mechanisms enabling faster proliferation can be very complex. Several genes can be involved in a trait and have synergistic effects. Such non-linear effects are summarized with the term epistasis. The selective advantage of a trait can also depend on the composition of the whole population (frequency-dependent effects). One prominent example of a frequency-dependent selective advantage is cooperation. Individuals — including microbes — can cooperate in many ways. This is especially true in biofilms [35]. One way is the secretion of public goods [36], [37]. In a population that involves cooperation, the success of the cooperative strategy depends on the frequency of cooperators and cheaters in the population [38] [39].

In population genetics, the evolutionary success of individuals is called their fitness. Fitness defines the rate at which individuals proliferate on average. For microbes fitness is basically their growth rate  $\alpha$ . For us the relation between the fitnesses of two strains is of particular interest. If strain  $A$  has a growth rate of  $\alpha_1$  and strain  $B$  grows at rate  $\alpha_2$ , the relative fitness of  $A$  compared to  $B$  is

$$f = \frac{\alpha_1}{\alpha_2}. \quad (1.1)$$

If  $\alpha_1 > \alpha_2$ , strain  $A$  has a selective advantage over strain  $B$  given by:

$$s = \frac{\alpha_1}{\alpha_2} - 1. \quad (1.2)$$

## 1.5. Sector patterns in microbial colonies

If both strains have the same growth rate,  $s$  is zero. We discuss the topic of selective advantages in growing biofilms in more detail in sections 1.5.3 and 2.9.

## 1.5. Sector patterns in microbial colonies

The type of microbial colonies we look at throughout this thesis is prepared as follows (see section 2.6 for details): Microbes are grown in liquid culture, cultures of different strains are then mixed, and a droplet of the mixture is placed onto an agar plate containing nutrients, that enable the microbes to grow and proliferate. Placing the droplet is called inoculation, and the resulting circular spot on the plate where the microbes have been placed is called the homeland. The agar plate is then incubated at appropriate temperature ( $37^{\circ}\text{C}$  for *E. coli* and  $30^{\circ}\text{C}$  for yeast, if not stated otherwise) for about 1–3 days. During incubation the microbes divide and form a circular colony growing radially outwards. Hence, colony growth is a range expansion starting from the homeland and colonizing more and more of the initially unoccupied area of the agar plate. In our case after a couple of days colony growth slows down strongly at a colony diameter of about 1.5–2 cm. The reason for this may be lack of nutrients or drying of the agar.

It is an experimental observation that the microbes only grow and proliferate in a relatively thin band at the colony front [40] (see Figure 3.3). Behind that band the cells, albeit still alive, cease growing. This is a great opportunity for experimental study of the colony growth — behind the front the colony is left unchanged and therefore makes up a "frozen time-record" of the colony's growth history.

### 1.5.1. Formation of sectors

In our experiments we inoculate mixtures of differently labeled strains. After colonies have formed, we monitor them with a fluorescence microscope. A sketch of what the resulting colonies look like is shown in Figure 1.1, Figure 1.4 shows a microscope image of a real colony. The two colors represent the two microbial strains. In the center of the colony one can see a circular region of a dense speckle pattern. This is the area of the inoculum, or the homeland. The speckle pattern is formed because the two strains were completely mixed in the liquid, and therefore the two strains were randomly distributed within the inoculum. But on the outside the colony exhibits lots of thin radial sectors of alternating color. These sectors are formed as a consequence of the range expansion. This phenomenon was first described by Hallatschek et al. in 2007 [3].

## 1. Introduction

The growing colony can be described as an advancing wavefront similar to the classic model of Fisher, Kolmogorov, Petrovskii and Piskunov (FKPP) [41] [42] [43]. The FKPP model describes the change of (cell) concentration  $c(x, t)$  via a reaction-diffusion-equation with logistic growth:

$$\frac{\partial c}{\partial t} = \underbrace{\alpha c(\kappa - c)}_{\text{logistic growth}} + D \underbrace{\frac{\partial^2 c}{\partial x^2}}_{\text{diffusion}}. \quad (1.3)$$

$\alpha$  here is the growth rate of the cells, and  $\kappa$  is the carrying capacity of the habitat — the maximum concentration it can hold. Rescaling the concentration via

$$u := \frac{c}{\kappa} \quad (1.4)$$

yields

$$\frac{\partial u}{\partial t} = \underbrace{\alpha \kappa}_{=:k} u(1 - u) + D \frac{\partial^2 u}{\partial x^2}. \quad (1.5)$$

The (minimum) speed of the resulting Fisher wave is:

$$v = 2\sqrt{kD}. \quad (1.6)$$

The situation is depicted in Figure 1.2, which is a sketch of a transverse section along the red line in Figure 1.1. At the colony front only few cells live and contribute to the range expansion. This situation constitutes a continual population bottleneck, and therefore stochasticity plays a major role. If, by chance, only blue cells live at a certain front position, all cells beyond will be descendants of these blue cells and therefore form a blue sector. The same holds for yellow sectors.

This experiment makes the reduction of genetic diversity due to the range expansion visually observable. In every sector one of the two fluorescence variants present in the initial population is lost; only one color survives. Figure 1.3 shows a comparison of the serial bottleneck in Lenski-type experiments and the continual bottleneck in growing colonies.

1.5. Sector patterns in microbial colonies

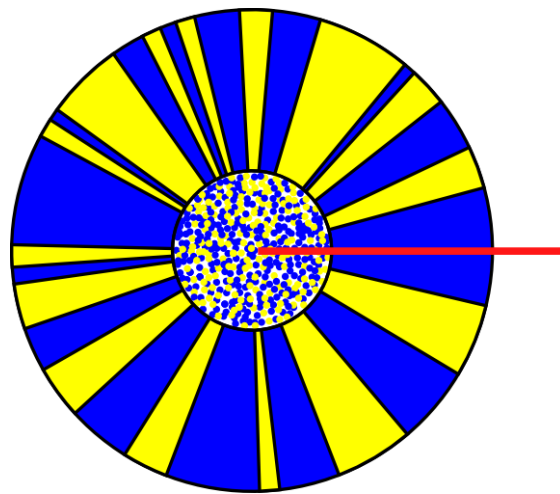


FIGURE 1.1.: **Sketch of a colony grown from a mixture of a blue and a yellow strain.** In the homeland (inner circle) blue and yellow patches are evenly distributed. Outside the homeland sectors of single color form. Cutting along the red line reveals the genesis of the sectors (see Figure 1.2).

1. Introduction

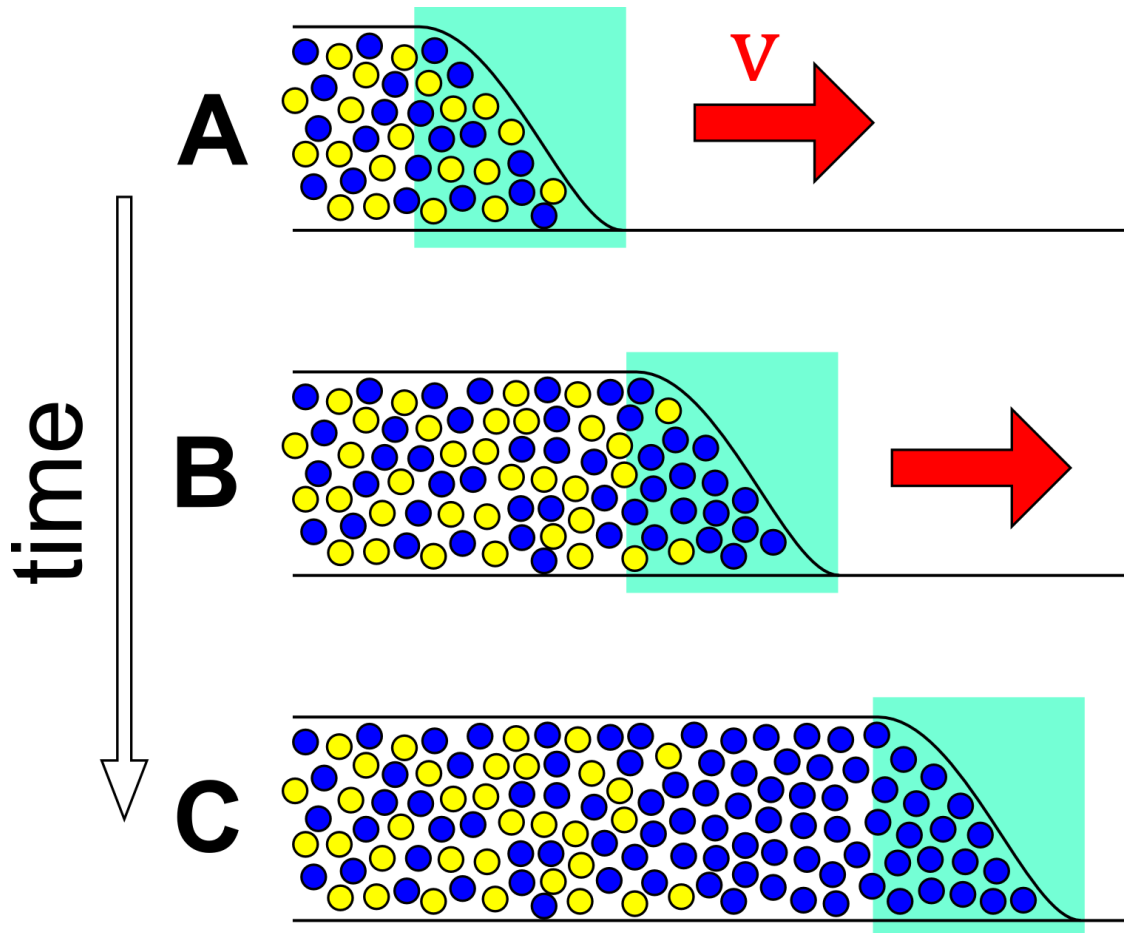


FIGURE 1.2.: **The moving edge of a growing colony.** A. Both strains are evenly distributed. B. By chance the tip of the wave now consists of almost only blue cells. C. The yellow cells have lost contact with the growing front. A completely blue sector has formed.

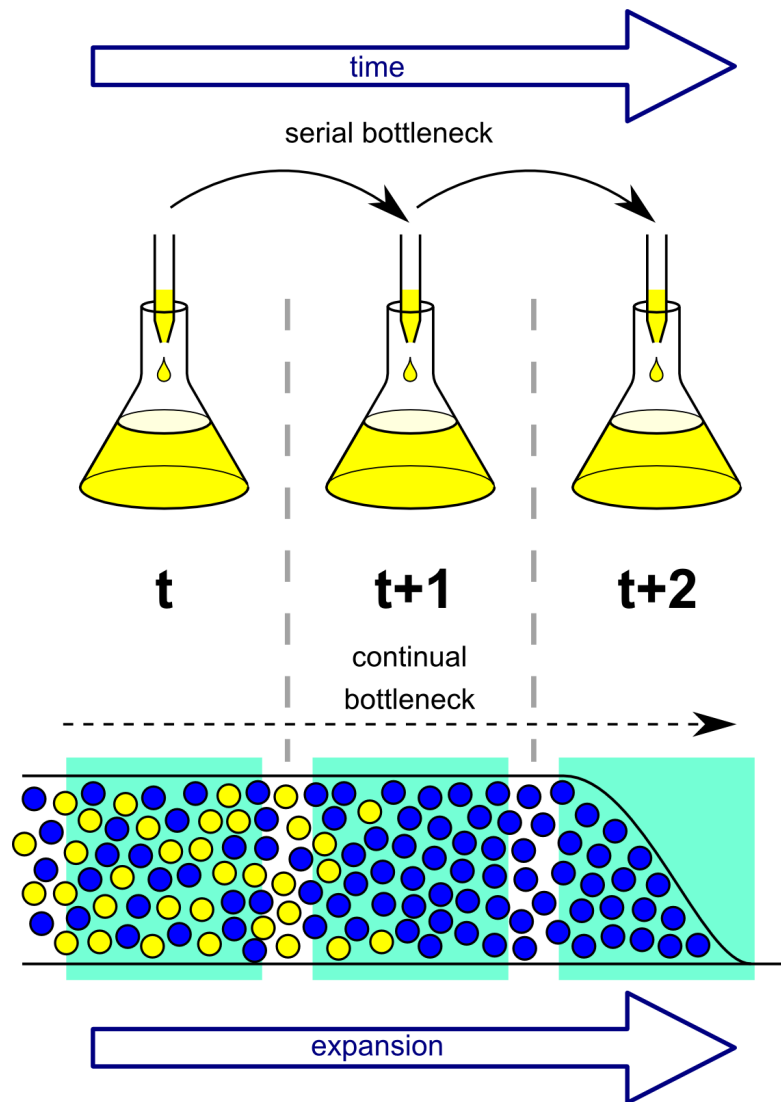


FIGURE 1.3.: Comparison between serial dilution of well-mixed populations and a continual bottleneck during a range expansion. Top: Lenski-type experiment. Microbes are grown in liquid. At discrete timepoints (e.g. every day) a sample of the liquid culture is transferred to fresh medium. This way a series of population bottlenecks is introduced. Bottom: colony experiment. Microbes are grown on a petri dish. The region of actively proliferating cells at the front moves forward continually. This leads to a continual population bottleneck.

## 1. Introduction

### 1.5.2. Difference between species

Both species mainly used in this work (*S. cerevisiae* and *E. coli*) exhibit characteristic sector patterns when grown on petri dishes (Figures 1.4 and 1.5). However, the patterns differ in two crucial aspects between these species. *E. coli* exhibits much fewer sectors than *S. cerevisiae*, and the boundaries between the sectors are much more ragged in the *E. coli* colony than the very straight sector boundaries in the *S. cerevisiae* colony. We discuss possible reasons for the different sector patterns in sections 2.4, 3.1 and 4.1.

It is sensible that the colony with more ragged boundaries ends up with fewer sectors: Two neighbouring boundaries are more likely to collide and separate the enclosed sector from the growing colony front. Hence, more sectors die out and fewer sectors reach the edge of the mature colony.

Figure 1.6 shows sector boundaries of an *E. coli* colony at higher magnification. The boundaries are zigzag lines. From the images one can estimate the typical length of a straight segment between to kinks to be on the order of  $50 \mu\text{m}$ . Hallatschek et al. presented a model in which the sector boundaries are described as random walks [3] [4]. The diffusion constant  $D$  of the random walk defines the raggedness of the sector boundaries. The straight sectors of *S. cerevisiae* exhibit a small diffusion constant, whereas the diffusion constant of *E. coli* sectors is large. Since this boundary diffusion determines the number of sectors that eventually survive, the diffusion constant is the measure of genetic drift in this system. *E. coli* exhibits high genetic drift — a high noise level — while genetic drift in *S. cerevisiae* is relatively small. Hallatschek et al. also investigated colonies of *P. aeruginosa* and found that they form sectors similar to *E. coli* [44].

Since the diffusion is caused by the cells pushing each other away, the diffusion constant in this system is proportional to the growth rate  $\alpha$  [45]:

$$D = \lambda\alpha. \tag{1.7}$$

The wave speed therefore is

$$v = 2\sqrt{kD} = 2\sqrt{\kappa\lambda\alpha^2} \propto \alpha. \tag{1.8}$$

Thus, the relative fitness of two strains  $A$  and  $B$  with growth rates  $\alpha_1$  and  $\alpha_2$ , respectively, defined in equation 1.1 becomes

$$f = \frac{\alpha_1}{\alpha_2} = \frac{v_1}{v_2}. \tag{1.9}$$

### 1.5. Sector patterns in microbial colonies

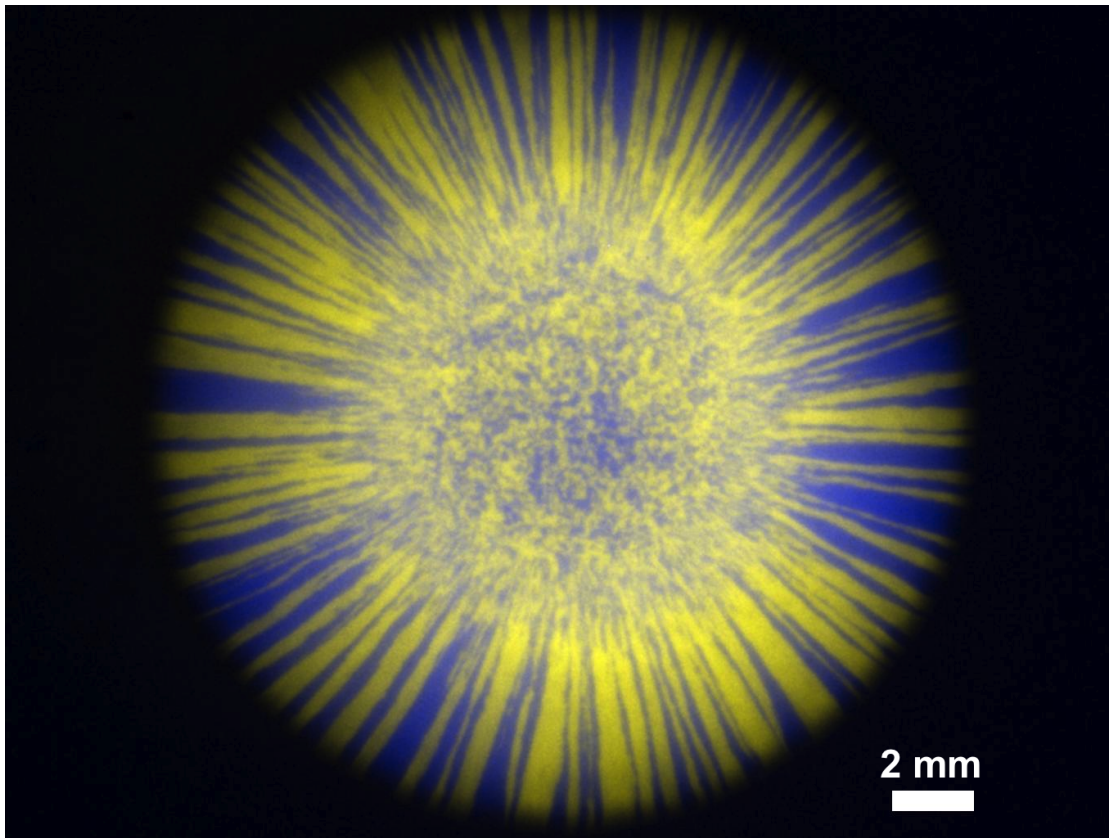


FIGURE 1.4.: **Fluorescent image of an *S. cerevisiae* colony (top view).** The colony was grown from a mixture of two differently labeled strains (shown here in blue and yellow). The speckle pattern in the center marks the area of the initial inoculum, the formation of the sectors on the outside is explained in the text.

This is very convenient, since expansion speeds are easier to measure in colony assays than growth rates. The corresponding selective advantage of  $A$  over  $B$  (equation 1.2) becomes

$$s = \frac{\alpha_1}{\alpha_2} - 1 = \frac{v_1}{v_2} - 1. \quad (1.10)$$

1. Introduction

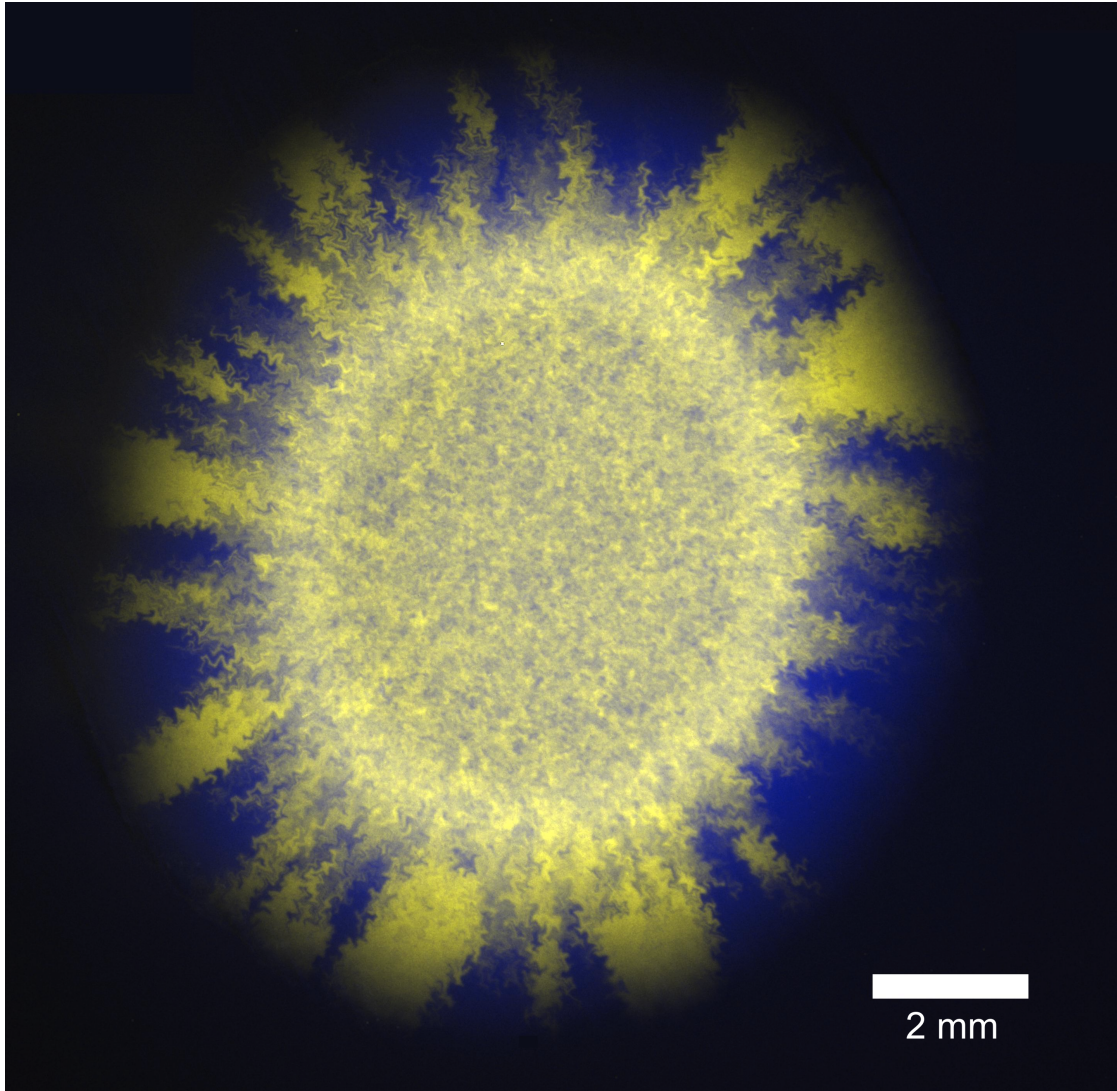


FIGURE 1.5.: **Fluorescent image of an *E. coli* colony (top view).** The colony was grown from a mixture of two differently labeled strains (shown here in blue and yellow). The speckle pattern in the center marks the area of the initial inoculum, the formation of the sectors on the outside is explained in the text.

1.5. Sector patterns in microbial colonies

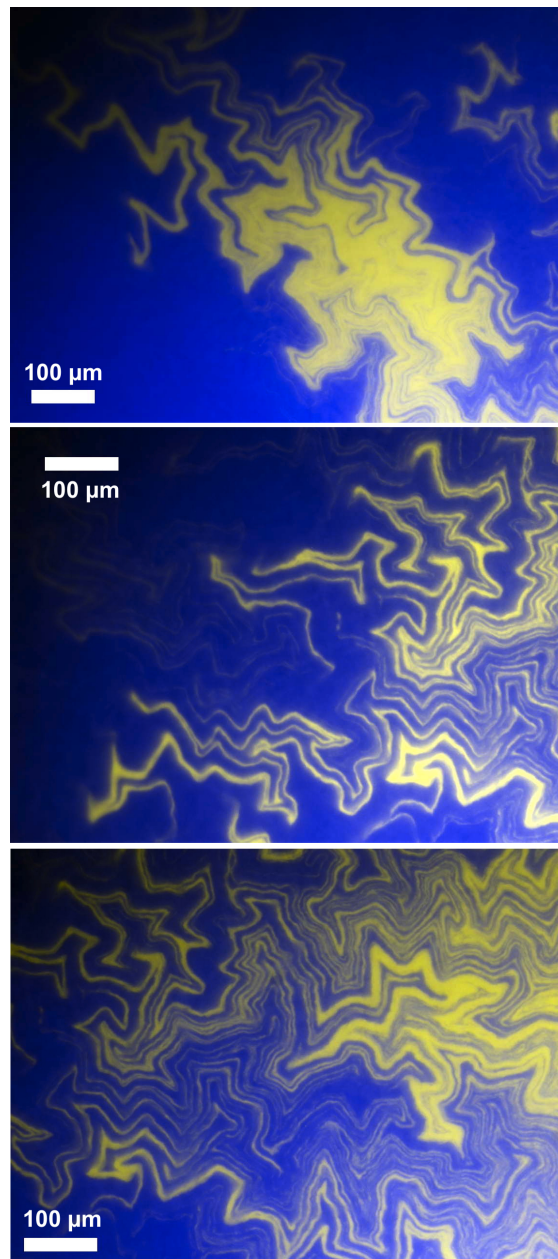


FIGURE 1.6.: Sector boundaries in a colony of *E. coli* (top view). Close-up of the colony shown in Figure 1.5. From the image we can roughly estimate the typical length between two kinks to be about  $50 \mu\text{m}$ .

## 1. Introduction

### 1.5.3. Natural selection

In this thesis we look at the interplay between genetic drift and natural selection. Figures 1.4 and 1.5 show colonies of strains without a fitness difference. In this case the sector boundaries are the result of unbiased random walks. If one of the strains had a fitness advantage relative to the other, the wavefront of this fitter strain would proceed faster. Therefore sectors of the fitter strain would not have a fixed angle but instead expand. The geometry of a sector produced by a strain with fitness advantage is explained in detail in section 2.9.

However, not every cell at the front eventually creates a sector. Many cells lose contact to the front due to genetic drift. Thus, in order to grow deterministically, the sector has to reach a certain size beyond that it will most likely survive genetic drift. We call this initial growth process the *establishment* of a sector. The central question of this thesis is, how likely it is for a beneficial mutation to get established. The establishment probability of a beneficial mutation has an impact on the adaptation speed of a species. Our approach to the central question is to grow colonies from a liquid culture that already contains fluorescently marked cells with a selective advantage. We then count the sectors these fitter cells produce. If the portion of mutant cells in the inoculum is low enough, so they form non-merging sectors, the number of established sectors is given by

$$n_{sec} = N_{mut} \cdot P_{est}, \quad (1.11)$$

$N_{mut}$  being the number of mutant cells at the front and  $P_{est}$  being the establishment probability. Alternatively, we can express the number of established sectors in terms of the total number of cells at the front  $N_{front}$

$$n_{sec} = p_{mut} \cdot N_{front} \cdot P_{est}, \quad (1.12)$$

$p_{mut}$  being the portion of mutant cells in the inoculum. The total number of cells able to actively take part in the range expansion is hard to determine. It not only depends on the total cell concentration in the inoculum, but also on the geometry of the inoculum. We would have to know the exact width of the active layer, as well as the exact height profile of the inoculum. The inoculum is not flat, but has a thick ring at the front due to the coffee-stain effect [46]. Furthermore, the establishment probability itself might depend on the total number of competing cells at the front. Thus, in this study we rather look at the *establishment rate* that we define as follows:

$$E := \frac{n_{sec}}{p_{mut}} = N_{front} \cdot P_{est}. \quad (1.13)$$

## 1.6. Aim of this study

Theory predicts the establishment rate to be proportional to the square-root of the selective advantage, and inversely proportional to the boundary diffusion constant [4]:

$$E \propto \frac{\sqrt{s}}{D}. \quad (1.14)$$

## 1.6. Aim of this study

Adaptation of microbes within a biofilm is a process of beneficial mutations entering the population, some of them getting established and growing to fixation. Overall the accumulation of these fixed beneficial mutations leads to a fitness increase of the population. Whereas the fixation of an established beneficial mutation can be viewed as a deterministic process, the establishment itself is stochastic — it is subject to genetic drift. Different species exhibit very different noise levels.

In this study we test what impact the observed difference in noise has on the establishment rate of beneficial mutations. We measure the rate at which beneficial mutations are established in colonies of different species. We show that establishment rates depend on the species and the growth temperature.

## *1. Introduction*

## 2. Materials and Methods

In this study we investigate, whether the observed differences in genetic drift lead to different establishment rates of beneficial mutations. In this chapter we describe the experimental methods used to conduct this investigation.

In section 2.1 we introduce the microbial strains that we used in our experiments, and in section 2.2 we give the composition of the necessary growth media.

The microscopy techniques used to image the sector patterns in microbial colonies are described in section 2.3. To observe how the patterns develop during colony growth we implemented time-lapse microscopy.

In our study we first looked for possible reasons for the differences in genetic drift between different species. Therefore we examined sector patterns of several microbial strains and found evidence that cell shape probably is an important factor, albeit not the only one. We explain our choice of strains for testing this in section 2.4.

One of our observations was that genetic drift in colonies also depends on the growth temperature. Since this might be linked with the cells' growth rate, in section 2.5 we present methods of measuring the growth rate at different temperatures, in liquid culture as well as in a colony.

So far we have no complete microscopic explanation for the differences in genetic drift between species and between growth temperature. But for the following main part of the study this does not matter, for we consider the different noise levels as a phenomenological parameter.

The main part of this study was the measurement of the establishment rates of beneficial mutations for different species and growth temperatures. We measured the establishment rates in colony assays, where we grew colonies from a mixture of two strains, one of which had a fitness advantage. These colony assays are explained in detail in section 2.6.

For analysing the colony assays it was crucial to determine the initial portion of mutant cells in the mixture. We present the method used to determine this portion in section 2.7.

In section 2.8 we explain how we calculated the establishment rate from the ratio of cell concentrations and the number of established sectors in the mature colonies.

## 2. Materials and Methods

Since the establishment rate should increase with the fitness advantage of the mutant strain [4], we measured the fitness difference between mutant and wild-type strain. Following simple geometric considerations, we were able to extract the fitness difference directly from the colony assays without the need of additional experimental setups. The geometric method for determining the fitness difference between the two strains directly from the sector patterns is described in section 2.9.

To make sure the observed strong differences between the measured establishment rates for different species are not due to variations in inoculation volume and total cell concentration, we performed two sets of control experiments. These experiments are described in section 2.10.

### 2.1. Microbial strains used in this study

The experiments in this study were conducted with a variety of strains. Table 2.1 shows an overview.

#### *E. coli*:

NEB were purchased from New England BioLabs [47]. REL606 and REL607 are the Ara<sup>-</sup> and Ara<sup>+</sup> ancestor strains from the Lenski experiment [16]. JE has a mutation in the *mrdA* gene leading to an unstable penicillin-binding protein PBP2 and spherical cell shape [48] [49] [50] [51] [52]. JE was provided by Waldemar Vollmer. SJ102 is an MG1655 strain equipped with YFP. SJ102 was provided by Ivan Matic.

All Strains of *E. coli*, except SJ102, were heat-shock transformed (see appendix A) using the plasmid pOH1 (YFP) or pOH2 (CFP), respectively [3]. These plasmids are based on the vector pTrc99A and contain the YFP/CFP gene under control of the *lac*-operon. The plasmids confer resistance to 0.1 g/L ampicillin and are inducible by 0.1 mM isopropyl  $\beta$ -D-thiogalactopyranoside (IPTG).

The strains marked with 'mut' carry spontaneous beneficial mutations. We observed them in colony experiments when they produced expanding sectors. We picked cells from the expanding sectors and cultivated them.

#### *S. cerevisiae*:

yNK-RFP is a W303 strain equipped with RFP. This strain was provided by Nilay Karahan. Paris-CFP and -YFP are K699 strains equipped with CFP/YFP respectively [3].

## 2.1. Microbial strains used in this study

Strain	Trait
<i>E. coli</i>	
NEB-YFP	rod-like NEB 5-alpha w/ pOH1
NEB-CFP	rod-like NEB 5-alpha w/ pOH2
NEB-CFP mut	beneficial mutation of NEB-CFP
REL606-YFP	rod-like Ara <sup>-</sup> ancestor w/ pOH1
REL606-CFP	rod-like Ara <sup>-</sup> ancestor w/ pOH2
REL607-CFP	rod-like Ara <sup>+</sup> ancestor w/ pOH2
SJ102	rod-like MG1655 w/ YFP
JE-YFP1	spherical w/ pOH1
JE-YFP4	spherical w/ pOH1
JE-YFP4 mut	beneficial mutation of JE-YFP4
JE-CFP4	spherical w/ pOH2
JE-CFP4 mut	beneficial mutation of JE-CFP4
<i>S. cerevisiae</i>	
yNK-RFP	ellipsoidal budding yeast W303 w/ RFP
Paris-YFP	ellipsoidal budding yeast K699 w/ YFP
Paris-CFP	ellipsoidal budding yeast K699 w/ CFP
<i>S. pombe</i>	
MJ95	rod-like fission yeast
M2	MJ95 w/ GFP

Table 2.1.: The microbial strains used in his study.

*S. pombe*:

MJ95 and M2 were provided by Marco Geymonat. M2 is derived from MJ95 and contains the integrative Leu1 plasmid SP4 expressing GFP under the promoter of Shk1.

Throughout this study we refer to pairs of strains by the abbreviations listed in Table 2.2. The fitter strain of a pair (in non-neutral pairs) is mentioned first.

## 2. Materials and Methods

Rod-like <i>E. coli</i>			
NEB	NEB-CFP mut	vs.	NEB-YFP
NEB neutral	NEB-CFP	vs.	NEB-YFP
REL	REL606-YFP	vs.	REL607-CFP
REL neutral	REL606-YFP	vs.	REL606-CFP
SJNEB	SJ102	vs.	NEB-CFP
Spherical <i>E. coli</i>			
JE41	JE-CFP4 mut	vs.	JE-YFP1
JE44	JE-YFP4 mut	vs.	JE-CFP4
<i>S. cerevisiae</i>			
Yeast	yNK-RFP	vs.	Paris-YFP
Yeast neutral	Paris-CFP	vs.	Paris-YFP
<i>S. pombe</i>			
POM neutral	MJ95	vs.	M2

Table 2.2.: Pairs of strains used in colony assays.

## 2.2. Growth media

If not stated otherwise, *E. coli* were grown in LB medium (lysogeny broth, also called Luria-Bertani), *S. cerevisiae* in YPD medium (yeast extract peptone dextrose) and *S. pombe* in YES medium (yeast extract with supplements).

Composition of LB:

Tryptone:	10 g/L
Yeast extract:	5 g/L
NaCl:	10 g/L

Composition of YPD:

YPD broth (Sigma Aldrich): 50 g/L

### 2.3. Microscopic imaging and time-lapse movies

Composition of YES:

Yeast extract:	5 g/L
Glucose:	30 g/L
Adenine:	225 mg/L
Histidine:	225 mg/L
Leucine:	225 mg/L
Uracil:	225 mg/L
Lysine hydrochloride:	225 mg/L

For producing agar plates, 15 g/L agar were added to the medium. Media were autoclaved after preparation. In case of LB, 0.1 g/L ampicillin and 0.0238 g/L IPTG (0.1mM) were added after autoclaving and cooling the media to 55°C in a waterbath.

## 2.3. Microscopic imaging and time-lapse movies

We used a Zeiss AxioZoom.V16 microscope with LED illumination (CL 9000 LED) for brightfield imaging and a metal-halide lamp (HXP 200 C) for fluorescence imaging. Images were taken with an AxioCam MRm camera. The objectives used were PlanApo Z 0.5x/0.125 FWD 114 mm for full-colony imaging and PlanNeoFluar Z 2.3x/0.57 FWD 10.6 mm for imaging sector boundaries in detail. Filter sets for fluorescence microscopy were 38 HE GFP, 46 HE YFP, 47 HE CFP and 63 HE RFP. To monitor the growth of a colony we recorded time-lapse movies using the Zeiss software ZEN pro. For time-lapse movies at 37°C we placed the petri dish onto a hotplate.

## 2.4. Testing the influence of cell shape on genetic drift

First we looked for possible reasons of the different noise in *S. cerevisiae* and *E. coli*. Since the different noise levels are linked to different sector geometry, it is sensible to look for geometric differences between the cells on the single-cell level. *E. coli* cells are rod-like and elongate axially during cell division, whereas *S. cerevisiae* cells are ellipsoidal. Thus, cell-shape could play a major role for sector pattern geometry and therefore genetic drift. To test the impact of cell-shape, we grew

## 2. Materials and Methods

colonies from to additional strains. The first one, *E. coli* JE, is a strain with a mutated *mrdA* gene. This gene encodes the penicillin-binding protein PBP2. The change in the *mrdA* gene leads to spherical cell shape [48] [49] [50] [51] [52]. Having a spherical strain of *E. coli* we also looked for a rod-like strain of yeast. For this study we used *Schizosaccharomyces pombe*, which is a fission yeast. It has rod-like cells that divide axially like *E. coli*. We grew colonies of these two types of strains and imaged the resulting sector patterns.

## 2.5. Growth curves

We observed that the sector patterns and therefore the noise level in microbial colonies changes with growth temperature. One obvious difference in growing at different temperatures is the growth rate. We quantified growth rates at different temperatures in three experimental setups that are described in the following paragraphs.

### 2.5.1. Liquid culture

We used this setup to monitor growth of *E. coli* strain NEB-YFP in liquid culture at 37°C and at room temperature. Cells were grown overnight in liquid culture. 100  $\mu$ L of overnight culture were added into 500 mL LB containing 0.1 g/L ampicillin in a sterile flask. Flasks were shaken throughout the growth measurement at 200 rpm at the respective temperature. At regular intervals samples of the culture were taken and cell concentrations were determined using a cell counter (Multisizer 3, Beckman Coulter).

### 2.5.2. Colonies

We used this setup to monitor growth of colonies of *E. coli* and *S. cerevisiae* at 37°C, 30°C and room temperature. Cells were grown overnight in liquid culture. We inoculated colonies on agar plates and incubated them at the respective temperature. Every 24 hours colonies were imaged with the microscope and put back into the incubator afterwards. To determine the growth speed of the colonies, we manually fitted circles around the colonies using the ZEN software and measured their diameter.

### 2.5.3. Time-lapse

With this method we measured the growth speed of colonies of *E. coli* strain NEB-YFP at 37°C and at room temperature. Cells were grown overnight in liquid culture. We inoculated a colony on an agar plate and placed it under the microscope. (For the measurement at 37°C we placed the petri dish onto a hotplate on the microscope stage.) We then recorded a time-lapse movie of the growing colony using the ZEN software. In the resulting movies we determined the positions of the colony front at different timepoints and calculated the front speed via linear regression.

## 2.6. Colony assays

### 2.6.1. General procedure

The general experimental procedure is illustrated in Figure 2.1. The two strains to compete were grown overnight in liquid culture. We checked if the cell concentrations of both cultures were of the same order of magnitude, using a cell counter (Multisizer 3, Beckman Coulter). If the concentrations differed at max by a factor of 2 we mixed the cultures in the desired volume ratios. The exact ratio of viable cell concentrations was measured a posteriori (see below). We then inoculated spots of 2  $\mu$ L of the mixture onto an agar plate to grow colonies. Agar plates were sealed with parafilm and then incubated for up to 3 days at 37°C (*E. coli*) or 30°C (*S. cerevisiae*, *S. pombe*), if not stated otherwise. After colonies had grown, we imaged them with the fluorescence microscope. Established sectors were then counted manually.

### 2.6.2. Systematic assays

First we had to check the approximate ratio of cell concentrations, at which mostly non-interfering established sectors could be observed. For finding that ratio, we mixed the two strains in a number of different volume ratios, separated by a factor of 10 each. We selected the ratio which fit our needs best and used several ratios of the same order of magnitude, with smaller differences between them, for the quantitative experiments.

## 2. Materials and Methods

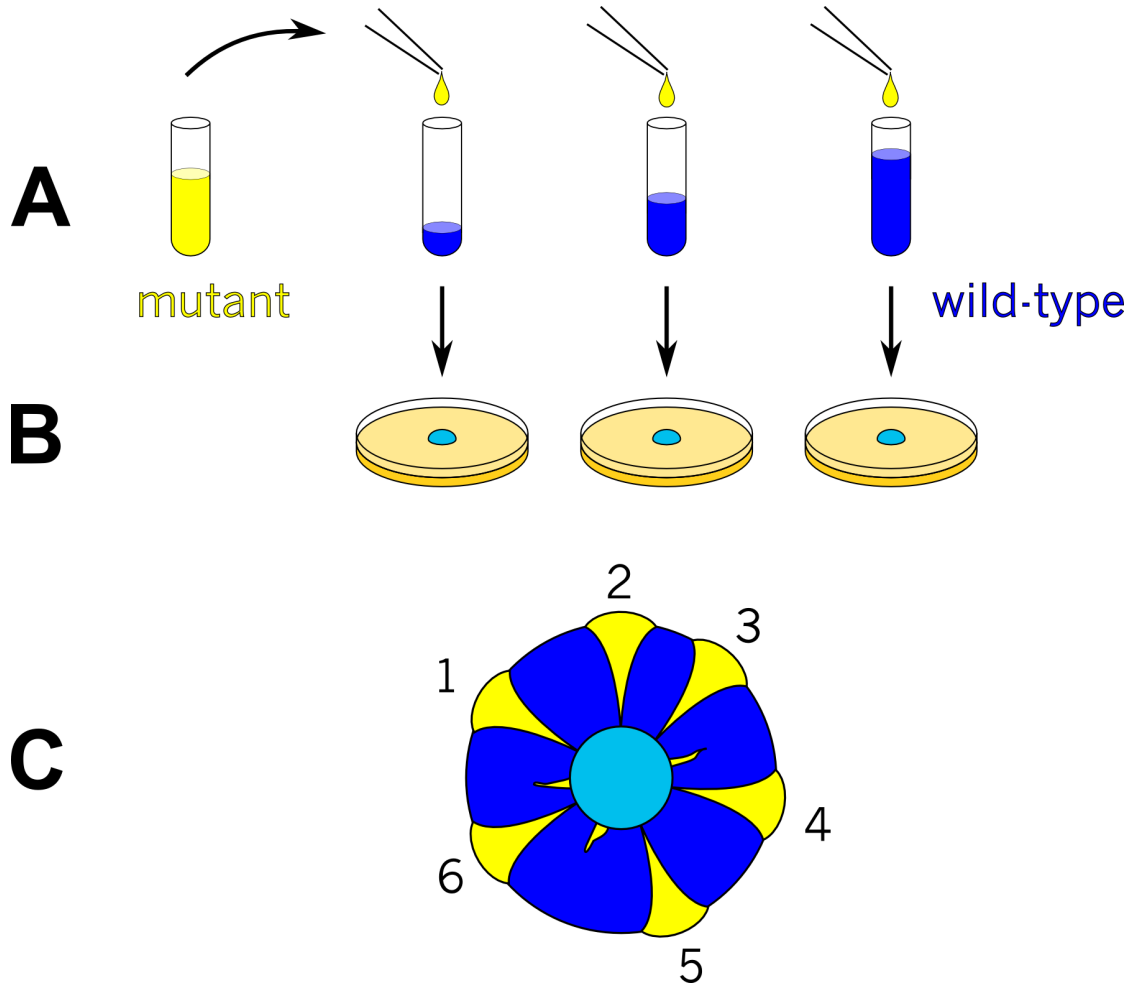


FIGURE 2.1.: **General experimental setup.** A) Two differently labeled strains are grown in liquid culture and then mixed in various volume ratios. B) Droplets of each mixture are inoculated onto agar plates with the appropriate nutrient medium. Plates are incubated at appropriate temperature until colonies have formed. C) Colonies are examined under the fluorescent microscope. established sectors of the mutant strain are counted. Sectors that die out behind the colony edge are not counted as established.

## 2.7. Determining initial portion of mutant cells

For the colony assays it is crucial to measure the initial strain-to-strain ratio of viable cells as precisely as possible <sup>1</sup>. Measuring the cell concentrations of the two strains independently and calculating the ratio afterwards is prone to systematic errors. Fortunately we can measure the ratio of viable cell concentrations directly thanks to the differing fluorescence colors used in our setup.

The two strains are grown separately overnight in liquid culture at appropriate temperature to saturation. The cell concentrations are estimated roughly with a cell counter (Multisizer 3, Beckman Coulter) to check, if both concentrations are of the same order of magnitude. The two liquid cultures are then mixed at desired volume concentrations for the colony assays (see section 2.6).

An additional mixture at volume ratio of 1:1 is made for determining the initial ratio of cell concentrations. The 1:1-mixture is diluted in pure growth medium by steps of 10 to final dilutions of  $10^{-4}$ ,  $10^{-5}$  and  $10^{-6}$ . Notice that the dilution does not change the ratio of viable cells.

For each of the final dilutions 2 to 4 agar plates of the appropriate growth medium are prepared. Onto each of the plates, 100  $\mu\text{L}$  of the diluted mixture is pipetted, then 5 to 10 autoclaved glass beads of 1 mm diameter are added. The lids are closed and the plates are shaken horizontally to distribute the cell solution evenly on the agar surface. It is important, that the glass beads touch every part of the surface and do not rotate at the rim of the petri dish instead. When all of the liquid has soaked into the agar, the lids are opened and the beads are poured out. The petri dishes are sealed with parafilm and incubated at appropriate growth temperature overnight.

The resulting colonies should be evenly distributed on the plate and not form any clusters. They are then examined with the fluorescence microscope. In our experiments the colors of the colonies can clearly be distinguished (Figure B.3). The colonies of each color are counted. For calculating the ratio of the cells, only plates with 20 to 200 colonies are used.

---

<sup>1</sup>The mutant portion  $p_{mut}$  and the mutant-to-wild-type ratio  $r_{m/w}$  are linked via

$$p_{mut} = \frac{1}{1 + \frac{1}{r_{m/w}}}. \quad (2.1)$$

## 2.8. Measuring the establishment rate

The main goal of this study is to measure the establishment rate for different species and different growth temperatures.

### 2.8.1. Sector numbers and mutant portion

For small mutant portions we expect the number of establishment events  $n_{sec}$  to be proportional to the fraction of mutant cells  $p_{mut}$  in the inoculum. Thus, the ratio  $E = n_{sec}/p_{mut}$  should be independent of  $p_{mut}$  and therefore be a reasonable measure for the establishment rate for the respective species at the given growth temperature. For high mutant portions more and more established sectors will merge and therefore the number of sectors will not grow further. Due to the merging,  $n_{sec}/p_{mut}$  then is no longer a reasonable measure for the establishment rate. So in our experiments we only use mutant portions low enough, so that the sectors are independent.

### 2.8.2. Estimation of errors in establishment rate $E$

The establishment rate  $E$  is the fraction of the sector number  $n_{sec}$  and the mutant portion  $p_{mut}$ . Both quantities contribute to the overall measurement error.

To estimate the variation of  $n_{sec}$ , we calculate the standard error for each set of experiments with equal mutant portion. When measuring  $p_{mut}$  as described in section 2.7, we assume that the colonies of the two colors are binomially distributed. We calculate the Clopper-Pearson confidence intervals for the binomial distribution. Combining both error estimates we obtain the error  $\sigma_{E_i}$  of  $E_i$  for each set of experiments with equal mutant portion.

In order to obtain one single data point for each set of experiments with equal strains and temperature we calculate the weighted average of the  $E_i$  over all mutant portions:

$$\langle E \rangle = \frac{\sum_i \frac{E_i}{\sigma_{E_i}^2}}{\sum_i \frac{1}{\sigma_{E_i}^2}}. \quad (2.2)$$

The corresponding error is given by:

$$\sigma_{\langle E \rangle} = \max \left( \sqrt{\frac{1}{\sum_i \frac{1}{\sigma_{E_i}^2}}}, \sqrt{\frac{\sum_i \frac{(E_i - \langle E \rangle)^2}{\sigma_{E_i}^2}}{(N-1) \sum_i \frac{1}{\sigma_{E_i}^2}}} \right), \quad (2.3)$$

$N$  being the number of experiments for the respective strains and growth temperature. The detailed calculation of errors is explained in appendix D.

## 2.9. Determining fitness differences

A major advantage of our experimental setup is that one can measure the fitness difference between the two strains directly from the microscope images of the competition colonies. Therefore it is not necessary to run an additional experiment for measuring fitness differences. The absolute growth rates of the two strains are not needed for evaluation. The connection between fitness advantage and shape of the resulting sector is illustrated in Figure 2.2 and will be discussed in the following. The method is described in detail in [45].

The colonies in our experiment are circular, but for sake of simplicity we first consider a linear colony with a proceeding front (Figure 2.2, top). This type of colony could be implemented experimentally by inoculation with a razor blade dipped in cell culture. The red star in the figure marks the point a beneficial mutation occurs. In our experiments this would be a spot on the edge of the homeland where an isolated mutant cell starts establishing a sector. The wild-type strain (blue) has growth rate  $\alpha$  and expands at speed  $v \propto \alpha$ . The mutant strain (yellow) has a fitness advantage of  $s$  over the wild-type strain. It therefore has growth rate  $\alpha^* = \alpha(1 + s)$  and expands at speed  $v^* \propto \alpha^*$ . The shape of the sector can be obtained by utilizing an equal-times argument. Any arbitrary point on the sector boundary is reached by both strains simultaneously. While the wild-type reaches the point by just expanding vertically, the mutant has to cover a larger distance, starting from the red star. Since both strains reach the point simultaneously, the distances travelled are proportional to the respective expanding velocities.

From Figure 2.2 we see that

$$v^{*2} = v^2 + v_{\perp}^2. \quad (2.4)$$

2. Materials and Methods

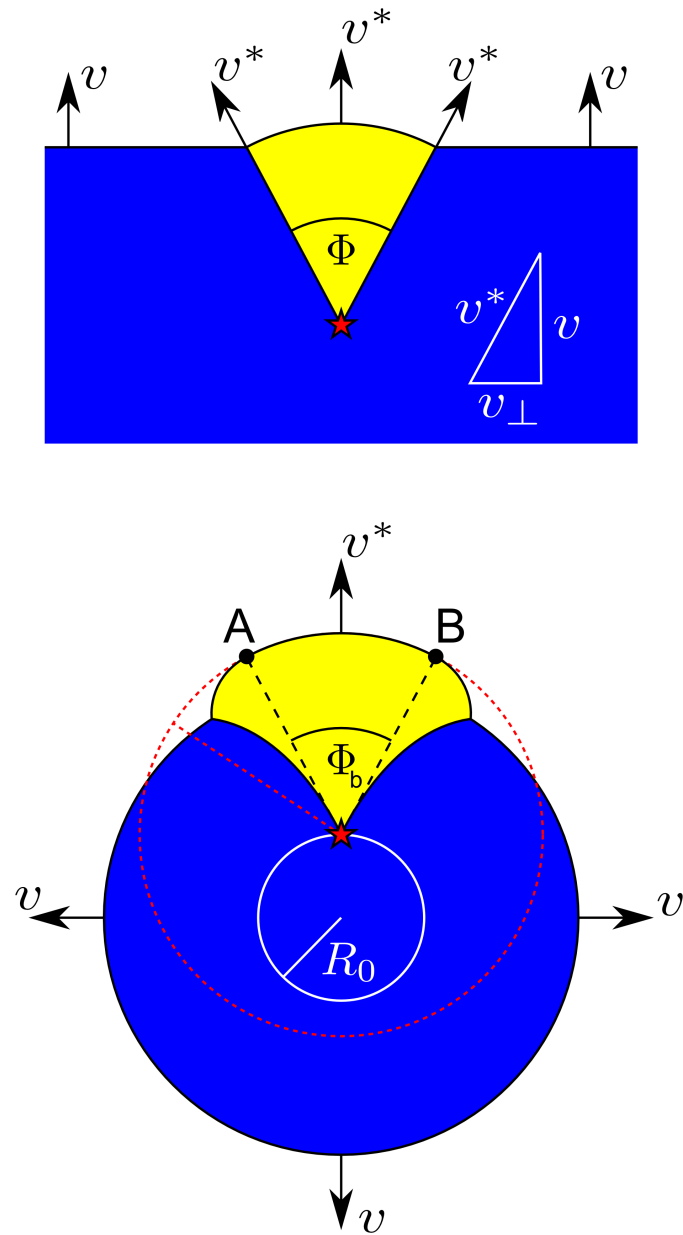


FIGURE 2.2.: **Sectors produced by strains with a fitness advantage.** The wild-type strain (blue) expands at speed  $v$ , the mutant strain (yellow) at higher speed  $v^*$ . Top: linear front. The mutant produces a sector of a circle. Bottom: circular front. Left and right boundary of the yellow sector are logarithmic spirals. The shape of the yellow sectors is calculated utilizing an equal-times argument (see text).

This leads to

$$\tan\left(\frac{\Phi}{2}\right) = \frac{v_{\perp}}{v} = \sqrt{\frac{v^{*2}}{v^2} - 1}. \quad (2.5)$$

Using equation 1.10 we conclude:

$$\tan\left(\frac{\Phi}{2}\right) = \sqrt{\frac{v^{*2}}{v^2} - 1} = \sqrt{\frac{\alpha^{*2}}{\alpha^2} - 1} = \sqrt{(1+s)^2 - 1} = \sqrt{2s + s^2} \quad (2.6)$$

Thus, we found the relation between the sector's opening angle and the selective advantage of the mutant. Note that no other properties of the system enter the equation.

Since in our experiments typical selective advantages do not exceed 30%, we can safely neglect the quadratic term and obtain

$$\tan\left(\frac{\Phi}{2}\right) = \sqrt{2s}. \quad (2.7)$$

In our experiments the geometry of the colony is different. We inoculate a circular droplet and obtain a circular colony (Figure 2.2, bottom). However, we still can calculate the sector shapes utilizing a similar equal-times argument.

Within the time increment  $dt$  the wild-type strain needs to proceed the radial distance  $dr$ , the fitter strain grows the longer distance  $dl$  along the sector boundary:

$$dt = \frac{dr}{v} = \frac{dl}{v^*}. \quad (2.8)$$

Expressing  $dl$  in polar coordinates  $(r, \phi)$ , the origin being the red star, we have:

$$\frac{dr}{v} = \frac{\sqrt{dr^2 + (rd\phi)^2}}{v^*}. \quad (2.9)$$

The solution reads [45]:

$$\phi(r) = \pm \sqrt{\frac{v^{*2}}{v^2} - 1} \cdot \ln\left(\frac{r}{R_0}\right). \quad (2.10)$$

The different signs correspond to the right and left boundary, respectively.  $R_0$  is the radial distance of the point of mutation or, in our experiments, the radius of the

## 2. Materials and Methods

homeland. The sector boundaries in this case are no straight lines but logarithmic spirals.

If the wild-type strain were not present, the mutant strain would form a circular colony centered around the red star (denoted by dotted red circle). Between points A and B on top of the yellow bulge, this circular shape is not disturbed by the wild-type strain. Within the sector of angle  $\Phi_b$  the mutant strain grows radially outwards. Beyond A and B, the front of the bulge is closer to the red star, for the mutant here has to expand along a curved line and not radially. Since the sector between A and B is the region of radial growth, the same relation between angle and fitness advantage as in the linear geometry holds:

$$\tan\left(\frac{\Phi_b}{2}\right) = \sqrt{\frac{v^{*2}}{v^2} - 1} = \sqrt{2s}. \quad (2.11)$$

This way one can obtain  $s$  from microscope images by fitting a circle to the bulge, determining A and B and measuring the enclosed angle. We placed the circle manually and measured the angle both using the ZEN pro software.

### 2.9.1. Estimation of errors in fitness advantage

We measured the fitness advantage of the mutant following the sector angle method described in section 2.9. For each combination of strains at a given temperature we analyzed 1 – 5 sectors and took the arithmetic mean of the measured angles,  $\Phi_b$ . We estimated the true angle to be within  $\Phi_b \pm 10^\circ$ .

## 2.10. Controls: varying inoculation volume and total cell concentration

The size of the inoculum varies; even when the same volume of liquid is pipetted onto the plate for inoculation in each experiment, the size of the resulting droplet is not always exactly the same. The number of established sectors might be dependent on the size of the inoculum, since a larger inoculum has a longer circumference and therefore a larger frontier. So more cells are initially at the front with the potential to form sectors. To make sure that our observed differences in sector numbers are not due to variation of the inoculum size, we had to check the influence of the size fluctuations. We inoculated a number of colonies with liquid volumes reaching from 1  $\mu\text{L}$  to 4  $\mu\text{L}$ . Directly after the droplets had dried, we imaged them with

### *2.10. Controls: varying inoculation volume and total cell concentration*

the microscope and measured the circumference. We then incubated the plates as usually and counted the resulting established mutant sectors.

As we did not fix the total cell concentration in the inoculum, but rather mixed the undiluted saturated overnight cultures and only determined the ratio of wild-type and mutant cell concentrations a posteriori, we had to check the effect of total cell concentration on the sector number. To do so, we mixed our liquid overnight cultures in the usual way. We then diluted the mixture 10-fold, 100-fold and 1000-fold. We inoculated droplets of all three dilutions as well as of the undiluted mixture. This way we could make sure that the mutant portion was the same in all of these experiments. We incubated the plates as usually and counted the resulting established mutant sectors.

## 2. *Materials and Methods*

## 3. Results

In this chapter we present the results of our study. In section 3.1 we show colony sector patterns generated by spherical *E. coli* and by the fission yeast *S. pombe*. We conclude that a rod-like cell-shape seems to be necessary for high-noise sector patterns, but it is not sufficient. We suggest that cell-to-cell adhesion also plays a major role.

Next we show the influence of growth temperature on genetic drift in microbial colonies in section 3.2.

In section 3.3 we show that the number of established mutant sectors in a colony is proportional to the portion of mutant cells in the inoculum for sufficiently low portions. We conclude that the ratio of sector numbers and mutant portion is indeed a valid measure for the establishment rate.

We show the establishment rates for the different strains and temperatures in section 3.4.

In sections 3.5 and 3.6 we present the results of our control experiments regarding inoculation volume and total cell concentration. We can show that none of these parameters explains the differences in establishment rates presented in section 3.4.

### 3.1. Influence of cell shape on genetic drift

In this part of the study we grew colonies from differently labeled pairs of spherical *E. coli* and rod-like *S. pombe*. Figure 3.1 shows a colony of spherical *E. coli* strains JE-YFP1 and JE-CFP4. One can see quite straight sector boundaries, like in the colonies of *S. cerevisiae*. Thus, spherical cell shape seems to promote straight sector boundaries.

Figure 3.2 shows a colony of rod-like fission yeast *S. pombe*. Sector boundaries are very straight, resulting in a large number of sectors. Therefore a rod-like cell-shape might be necessary, but is not sufficient for producing ragged sector boundaries.

### 3. Results

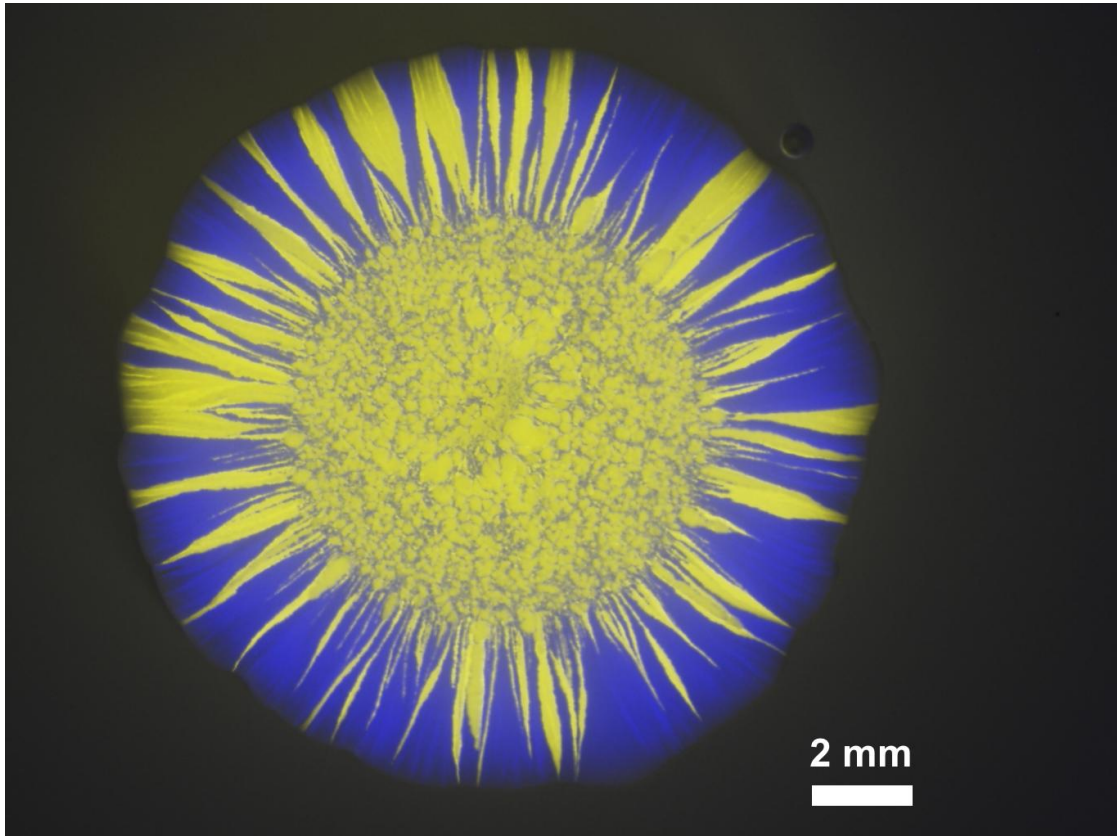


FIGURE 3.1.: **Fluorescent image of a colony of the spherical *E. coli* mutant JE (top view).** Sectors are rather straight, as in colonies of *S. cerevisiae*. In this colony most blue sectors expand and supersede the yellow ones. Thus, the blue strain obviously has a (small) fitness advantage over the yellow one.

3.1. Influence of cell shape on genetic drift

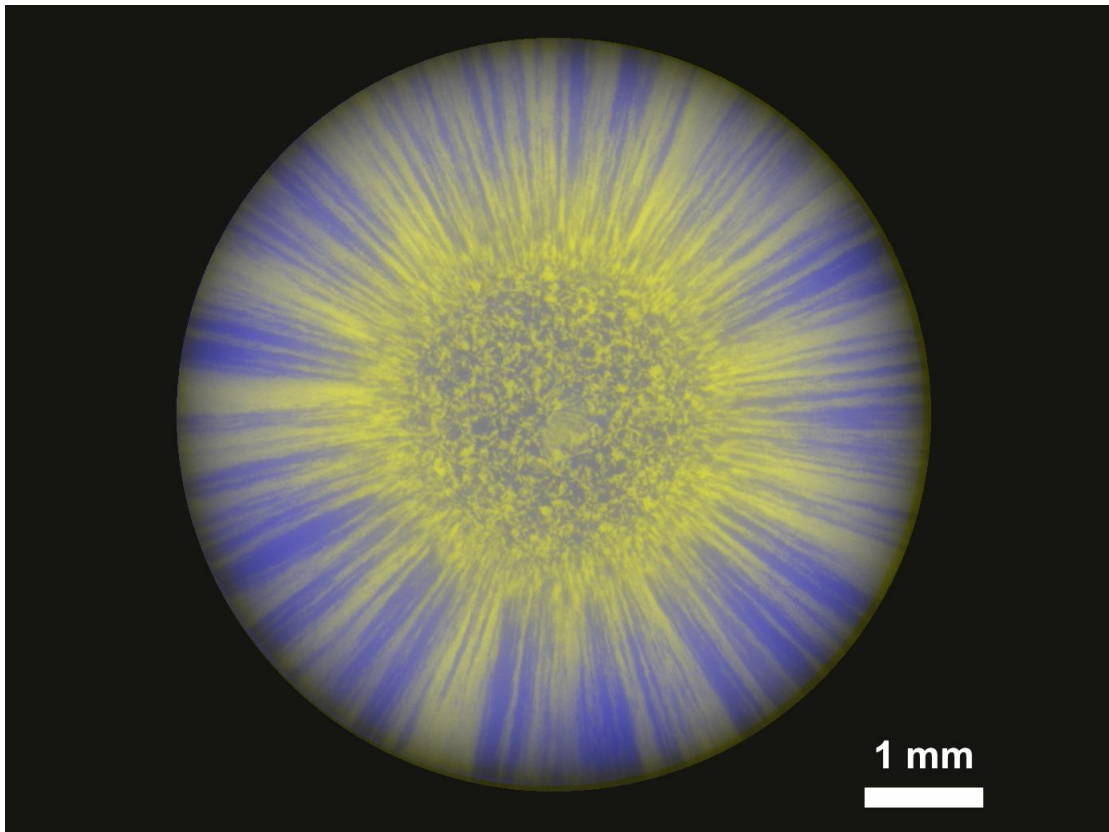


FIGURE 3.2.: Colony of rod-like fission yeast *S. pombe* (top view). Like in colonies of *S. cerevisiae*, a large number of sectors with very straight boundaries is formed.

### 3. Results

Figure 3.3 shows the front of a growing NEB colony as frames of a time-lapse recording. One can see how eventually all but one of the blue sectors lose contact to the front. The interesting feature of this time-series is that it shows how the sectors are folded into each other during growth. Longitudinal alignment of cells along tens of cell diameters probably is the crucial feature in the high-noise sector patterns of *E. coli*. Cell-to-cell adhesion or nematic order under pressure are possible reasons for the alignment. The typical length scale between two kinks estimated in section 1.5.2 probably can be explained by a buckling instability [53].

### 3.1. Influence of cell shape on genetic drift

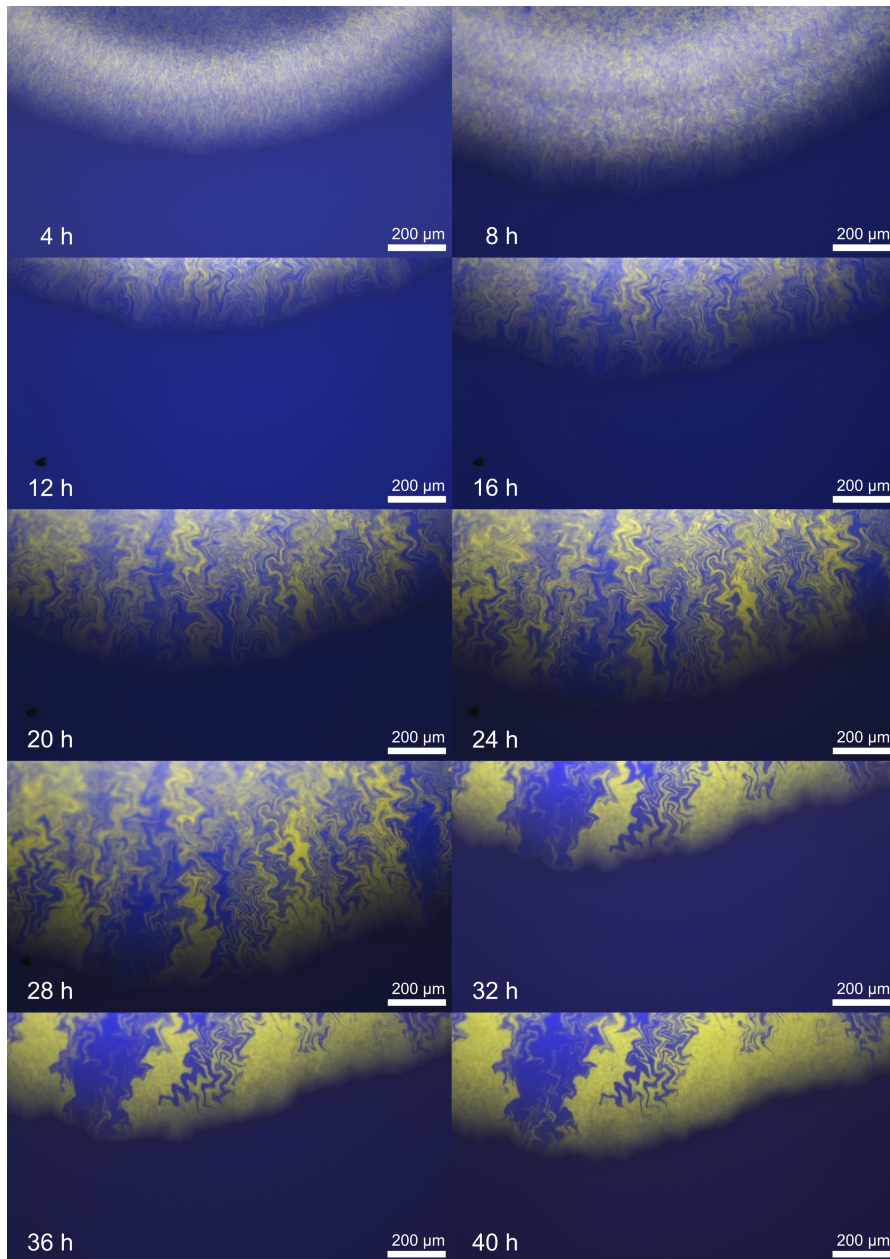


FIGURE 3.3.: **Growth of a colony of rod-like *E. coli* strain pair NEB neutral.** Images were extracted from a time-lapse movie recorded with ZEN software. Timestamps denote time after inoculation. To keep the growing front in the field of view, the microscope stage was adjusted between 8h and 12 h, as well as between 28 h and 32 h.

## 3.2. Influence of growth temperature on genetic drift

Figure 3.4 shows colonies grown from NEB and REL at three different temperatures. One can see that in both strains the number of sectors increases with decreasing temperature. Therefore genetic drift can be manipulated by tuning growth temperature. This is a great opportunity, since it allows us to measure establishment rates at different noise levels within the same species. This way all possible impacts of phylogenetic differences between species on establishment rates can be excluded.

One can speculate about the reason for the different noise levels at different growth temperatures. The most obvious effect of changing the temperature is different growth speed. In this study we measured growth rates in liquid culture as well as in colonies.

### 3.2.1. Liquid culture

Figure 3.5 shows the growth curves of NEB-YFP in liquid culture at 37°C and at room temperature. At 37°C one can see the typical sigmoidal bacterial growth behavior (lag phase, exponential phase and stationary phase) [54]. At room temperature the growth rate is drastically lowered. Here, the measured data points only cover a part of the exponential phase.

During exponential phase, the cell concentration grows according to

$$\frac{c(t)}{c(0)} = e^{\beta t} = e^{t/\tau} = 2^{t/T_2} \quad (3.1)$$

In this equation  $\beta$  is the exponential population growth rate, also named the Malthusian parameter.  $\tau = 1/\beta$  denotes the respective characteristic time, and  $T_2 = \tau \ln(2)$  is the mean doubling time. The parameter  $\beta$  was determined from data by linear regression of the logarithm of the cell concentration.

Temperature	$\beta / \text{h}^{-1}$	$\tau / \text{h}$	$T_2 / \text{h}$
37°C	$1.10 \pm 0.04$	$0.91 \pm 0.03$	$0.63 \pm 0.02$
RT	$0.35 \pm 0.01$	$2.86 \pm 0.08$	$1.98 \pm 0.06$

3.2. Influence of growth temperature on genetic drift

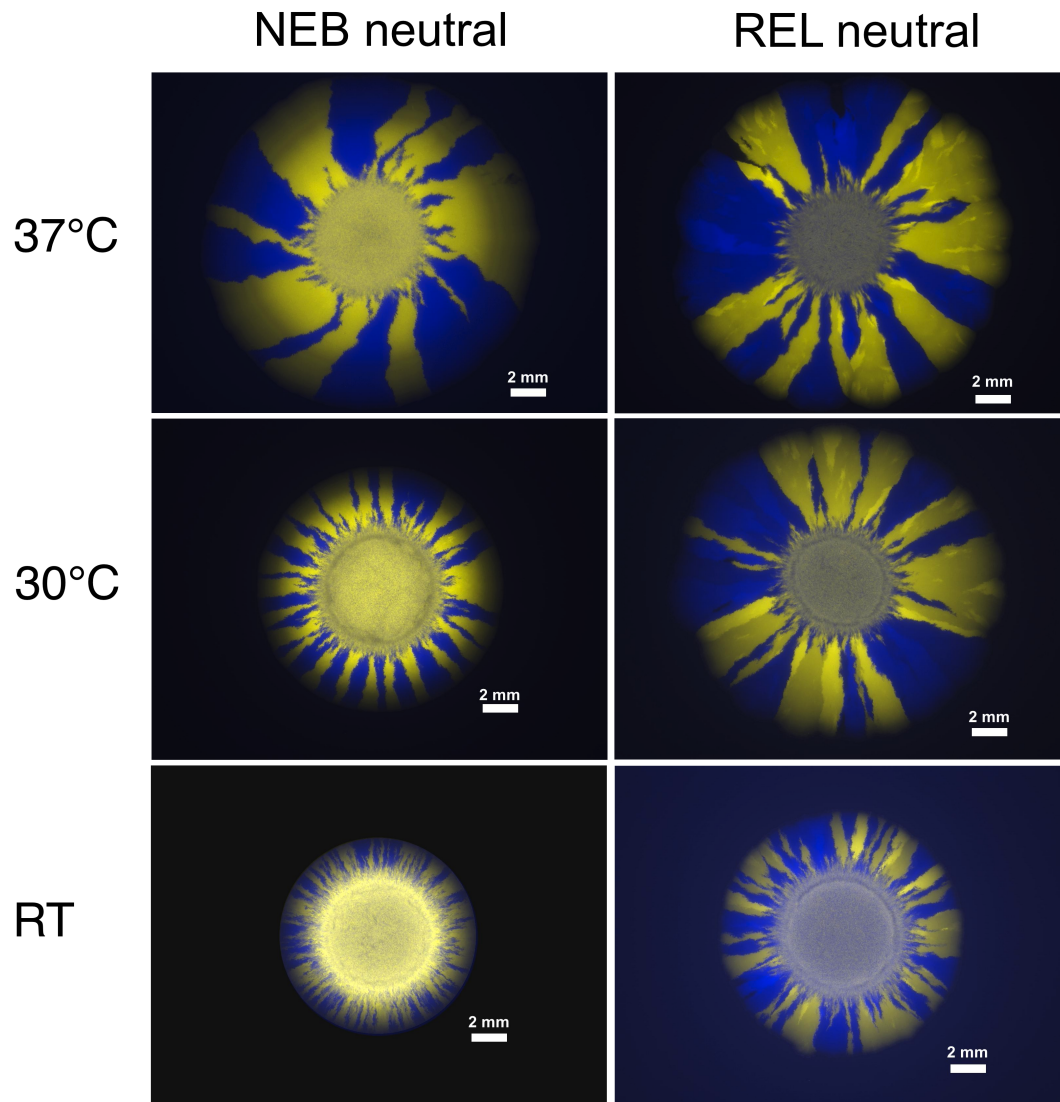


FIGURE 3.4.: Colonies of *E. coli* grown at 3 different temperatures. At room temperature, the number of sectors is distinctly larger than at the normal growth temperature of 37°C. All colonies have been incubated for 7 days.

### 3. Results

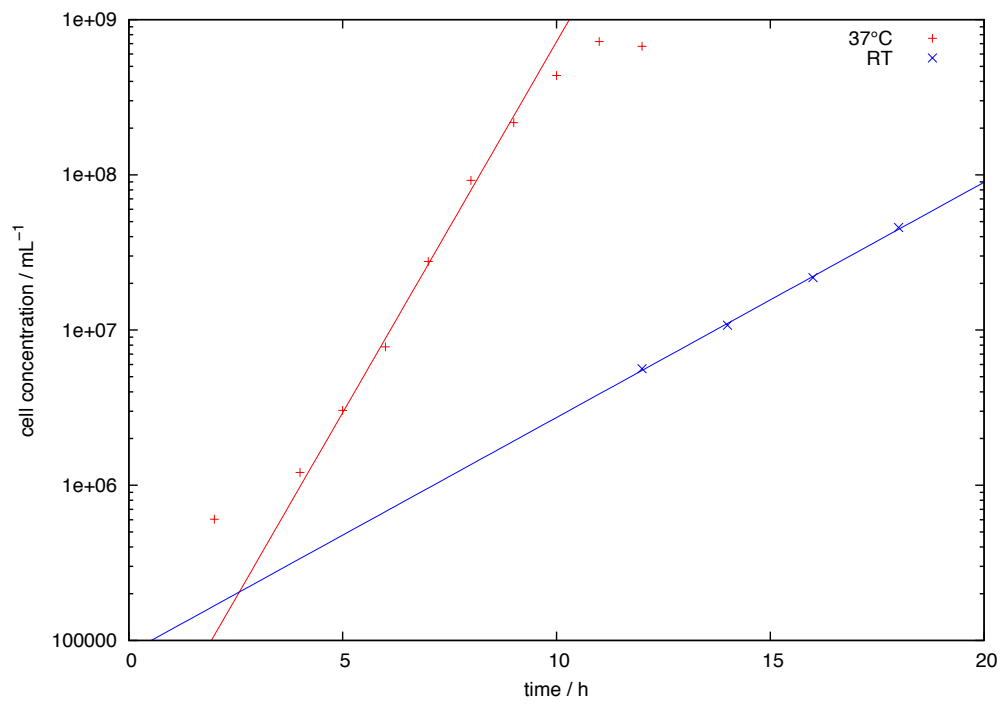


FIGURE 3.5.: **Growth curves of the *E. coli* strain NEB-YFP in liquid culture.** At 37°C one can see the typical sigmoidal growth behavior. At room temperature growth is drastically slowed down. Here the measured data points only cover a part of the exponential phase.

### 3.2. Influence of growth temperature on genetic drift

At room temperature the doubling time is more than three times as large as at 37°C.

#### 3.2.2. Colonies

Figure 3.6 shows growth curves of the NEB neutral pair at three different temperatures acquired via the colony method described in section 2.5.2. Figure 3.7 shows growth curves of the Yeast neutral pair at the same three temperatures. At 37°C and at 30°C NEB as well as Yeast grew at constant speed for 2–3 days after inoculation and then slowed down. At room temperature both strains exhibited a lag phase after inoculation. NEB had a lag phase of about 3 days and then grew at constant speed until at least 7 days after inoculation. Yeast had a lag phase of about 1 day and then grew at constant speed until at least 7 days after inoculation. We determined the colony front speeds by linear regression in the phases of constant growth speed.

Strains	Temperature	Front speed / $\mu\text{m h}^{-1}$	Front speed / $\mu\text{m d}^{-1}$
NEB	37°C	$39.8 \pm 1.5$	$954 \pm 36$
NEB	30°C	$27.4 \pm 0.1$	$658 \pm 2$
NEB	RT	$13.3 \pm 0.3$	$319 \pm 6$
Yeast	37°C	$27.9 \pm 0.7$	$669 \pm 17$
Yeast	30°C	$34.3 \pm 0.0$	$822 \pm 0$
Yeast	RT	$18.3 \pm 0.3$	$438 \pm 7$

Note that the front speed is only half the slope in the graphs, since there we show colony diameters and not radii. NEB grows optimally at 37°C, Yeast at 30°C. At room temperature both species grow much slower.

### 3. Results

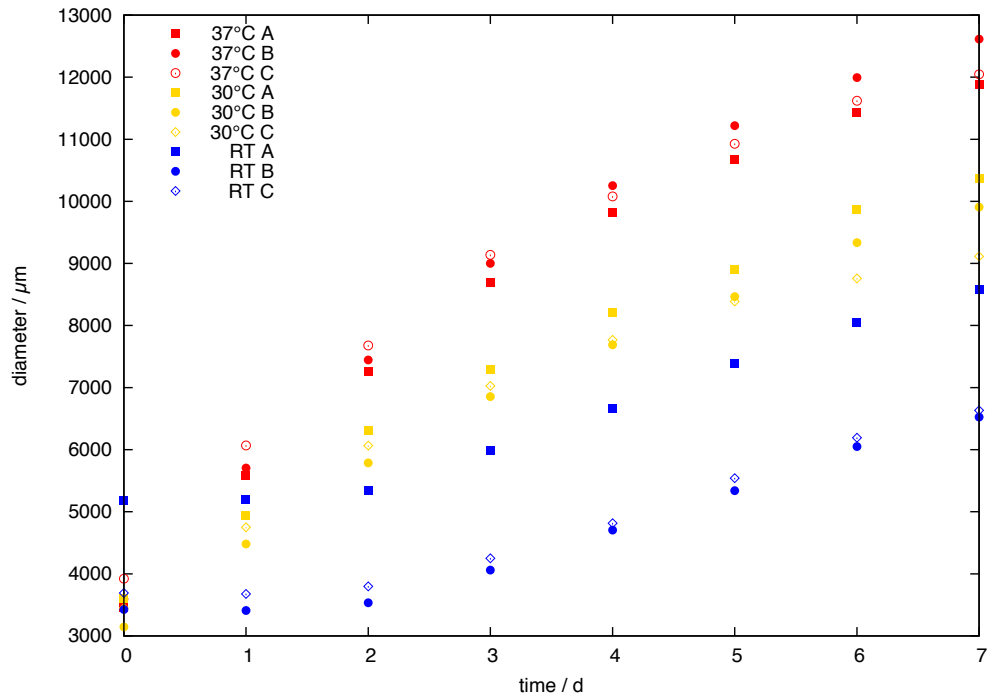


FIGURE 3.6.: Growth curves of the *E. coli* strain pair NEB neutral obtained via the colony method. At each of the 3 temperatures, 3 colonies were grown and analyzed (A, B and C). At 37°C and at 30°C, colonies grew at constant speed for 2–3 days after inoculation and then slowed down. At room temperature, colonies exhibited a lag phase of about 3 days and then grew at constant speed until at least 7 days after inoculation.

### 3.2. Influence of growth temperature on genetic drift

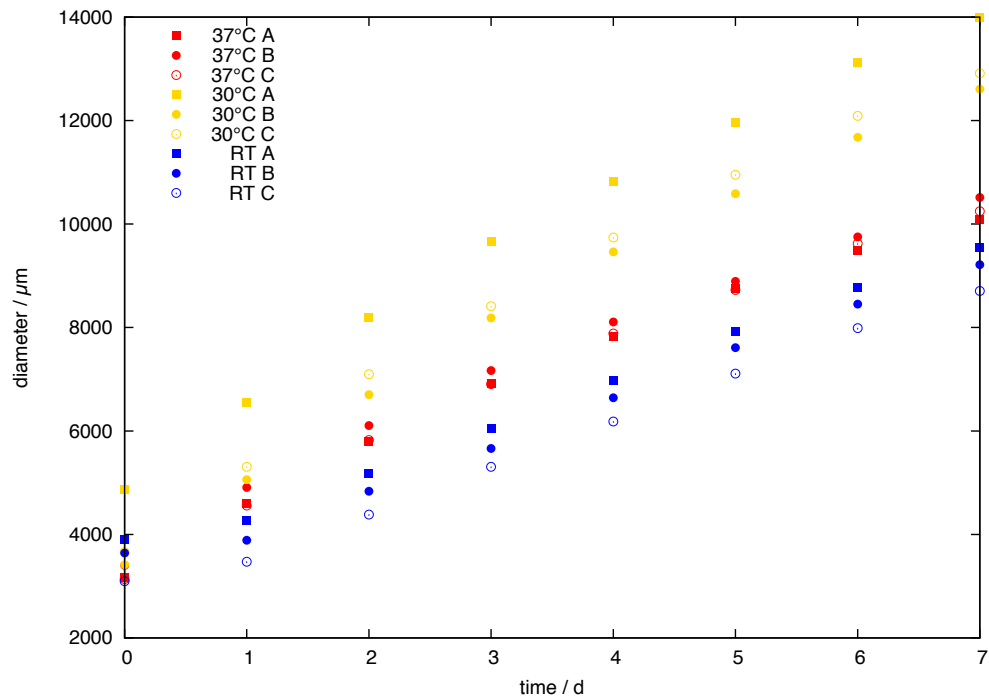


FIGURE 3.7.: **Growth curves of the *S. cerevisiae* strain pair Yeast neutral obtained via the colony method.** At each of the 3 temperatures, 3 colonies were grown and analyzed (A, B and C). At 37°C and at 30°C, colonies grew at constant speed for 2–3 days after inoculation and then slowed down. At room temperature, colonies exhibited a lag phase of about 1 day and then grew at constant speed until at least 7 days after inoculation.

### 3. Results

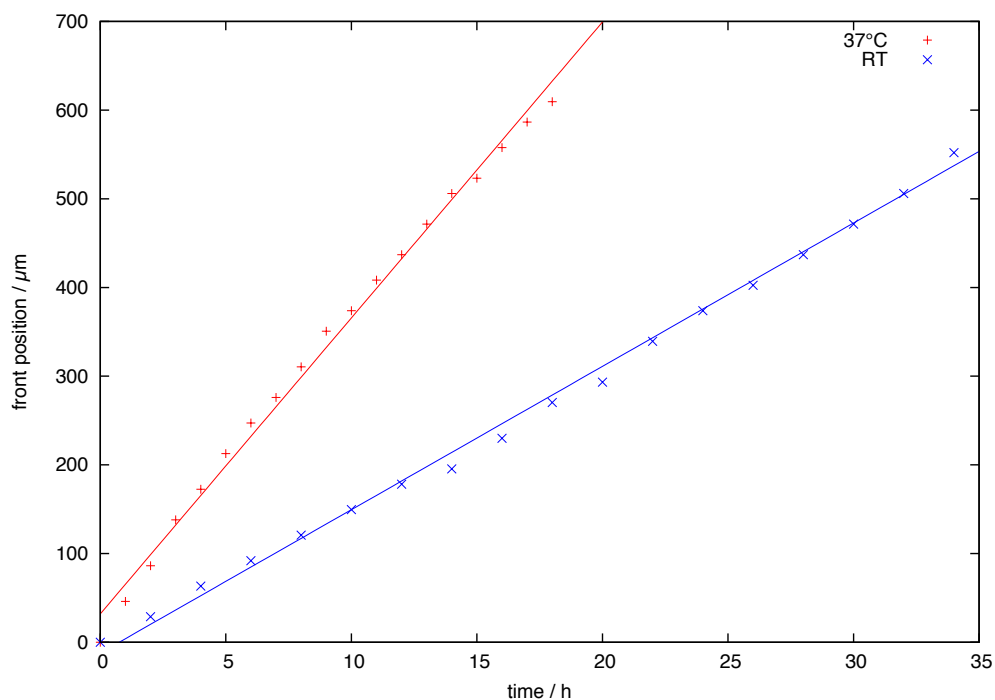


FIGURE 3.8.: **Growth curves of the *E. coli* strain pair NEB neutral obtained via the time-lapse method.** At both temperatures the front proceeds at constant speed. As well as in liquid culture, growth at room temperature is slower than at 37°C.

#### 3.2.3. Time-lapse

Figure 3.8 shows the advance of the colony front of the NEB neutral pair measured via the time-lapse method described in section 2.5.3. For each temperature one colony was analyzed. Speeds were obtained via linear regression.

Strains	Temperature	Front speed / $\mu\text{m h}^{-1}$	Front speed / $\mu\text{m d}^{-1}$
NEB	37°C	$33.4 \pm 0.6$	$801.6 \pm 14.4$
NEB	RT	$16.2 \pm 0.2$	$388.8 \pm 4.8$

### *3.2. Influence of growth temperature on genetic drift*

The front speeds are in good agreement with the ones measured via the colony method. One reason for the slightly slower growth at 37°C in the time-lapse method might be the temperature gradient created by the hotplate. The temperature on top of the agar plate was probably a bit lower than 37°C.

### 3.3. Sector number is proportional to initial mutant portion

Figure 3.9 shows the number of established sectors versus the mutant portion in the inoculum for all of our experiments with low mutant portion. As one can see, the data indeed show a linear dependence of sector number on the initial mutant portion.

Since for low mutant portions  $p_{mut}$  the number  $n_{sec}$  of established sectors is proportional to  $p_{mut}$ , the quotient

$$E = \frac{n_{sec}}{p_{mut}} \quad (3.2)$$

is independent of  $p_{mut}$  in this case. Therefore  $E$  is indeed a reasonable measure for the establishment of mutant sectors.

In the next section we compare the establishment rates for the different experimental scenarios, especially for the different species — those with high and those with low genetic drift. Since  $E$  depends on the fitness advantage  $s$  of the mutant strain, in Figures 3.12, 3.13 and 3.14 we plot  $E$  as a function of  $s$ .

### 3.3. Sector number is proportional to initial mutant portion

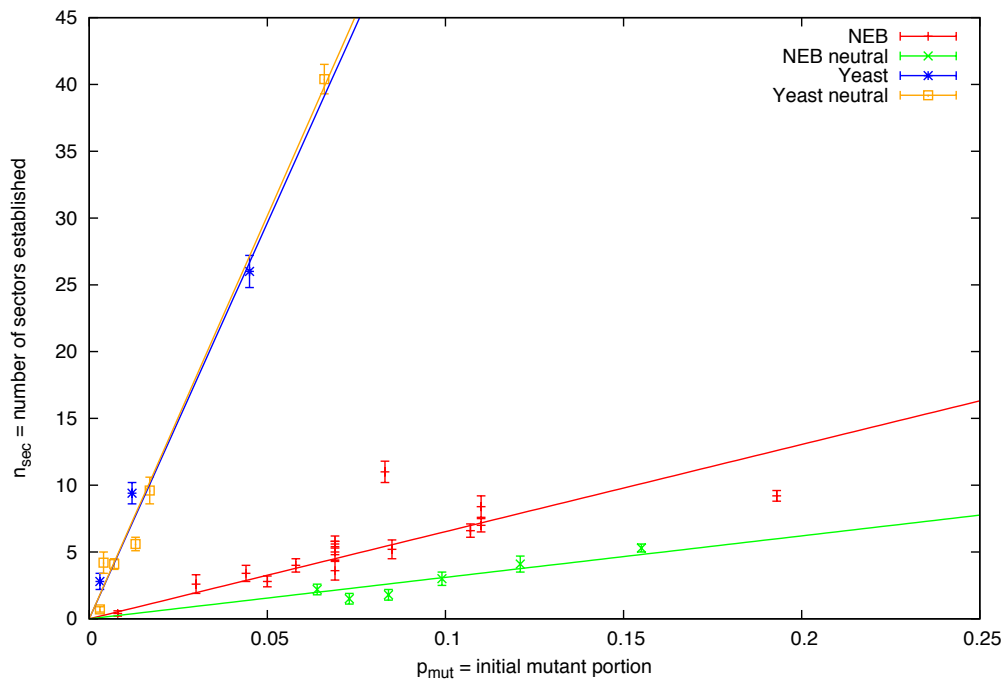


FIGURE 3.9.: **Established sectors versus initial mutant portion.** *E. coli* colonies were grown at 37°C, *S. cerevisiae* colonies at 30°C. Vertical errorbars indicate the standard error. Data were fitted via linear regression with one parameter (slope).

### 3. Results

#### 3.4. Establishment rates for different species and different growth temperatures

In section 1.5 we have shown microscope images of colonies grown from strains with equal fitness. In section 2.9 we have explained how sectors of strains having a selective advantage look like. Here we present microscope images of sectors established by fitter strains. Figure 3.10 shows a colony of rod-like *E. coli* in which the fitter strain has produced 4 sectors. Figure 3.11 shows a colony of *S. cerevisiae* in which the fitter strain has produced 15 sectors. As in the neutral case, the sectors of *S. cerevisiae* have much straighter boundaries and therefore their logarithmic-spiral-shape can nicely be seen.

3.4. Establishment rates for different species and different growth temperatures

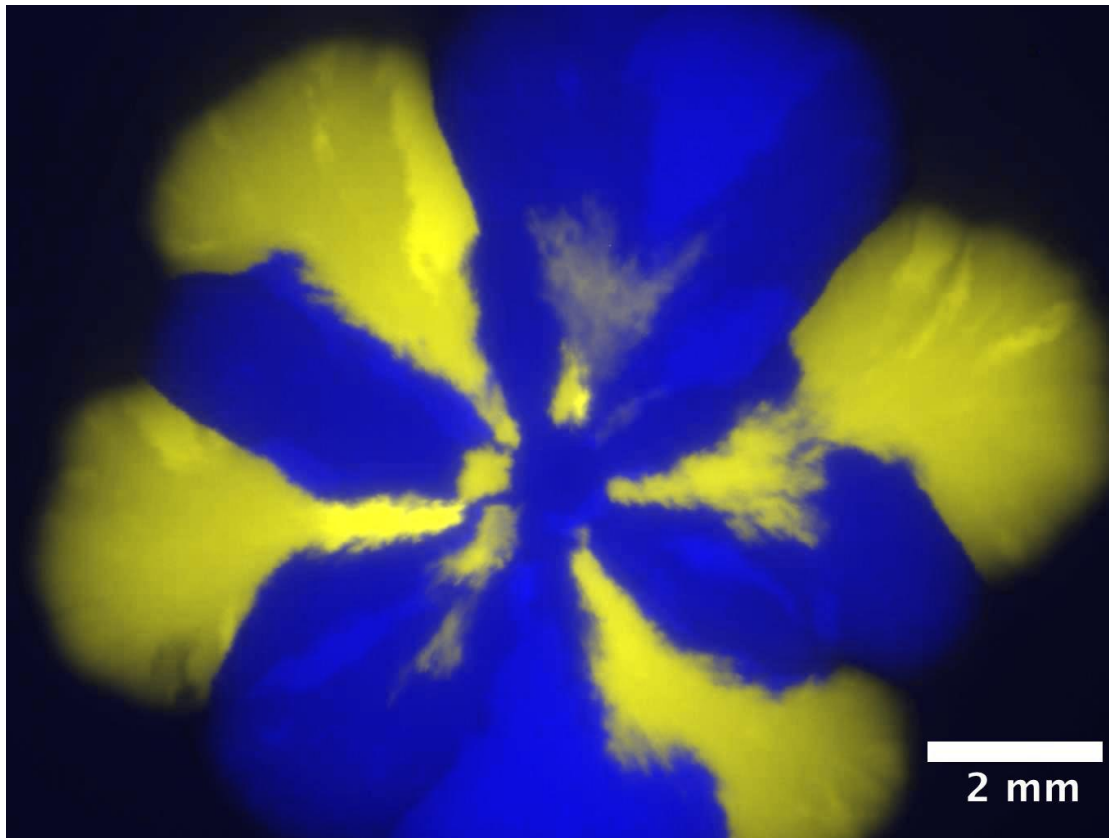


FIGURE 3.10.: Established sectors of rod-like *E. coli* strain pair REL. REL607-CFP is shown in blue, the fitter strain REL606-YFP is shown in yellow. The initial portion of REL606-YFP in this case was 16 %.

### 3. Results

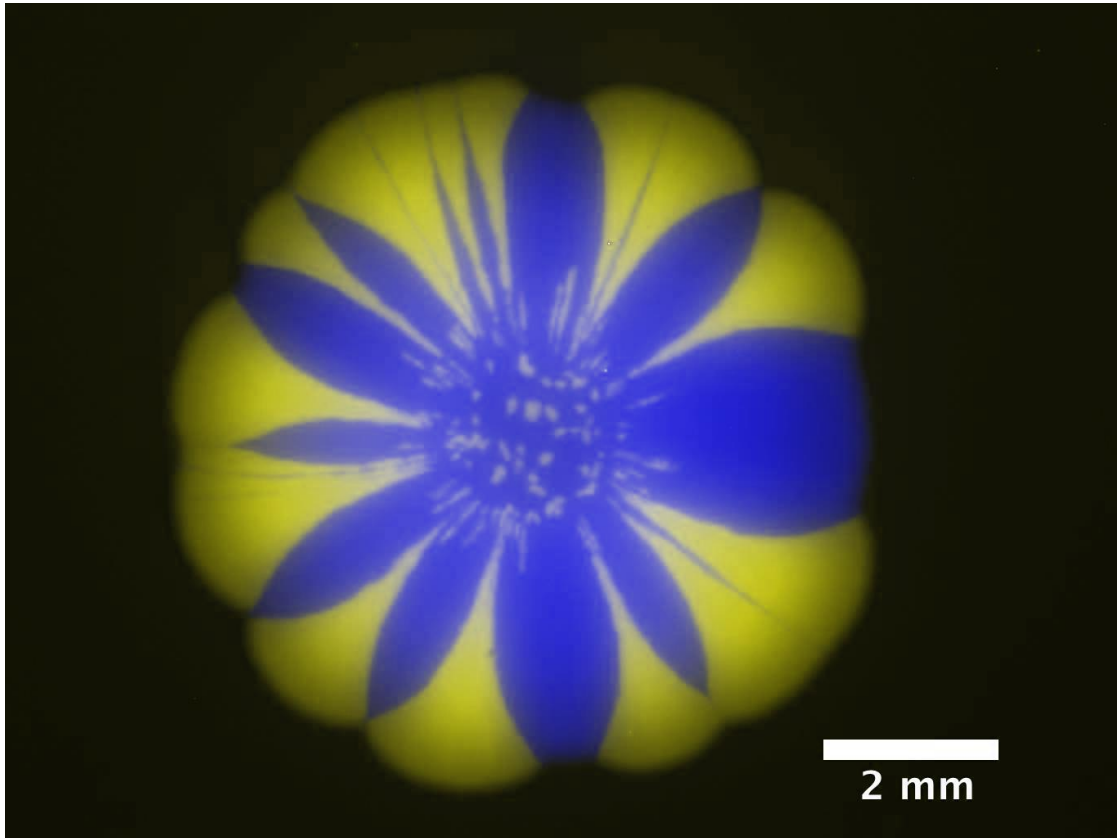


FIGURE 3.11.: **Established sectors of *S. cerevisiae* strain pair Yeast.** Paris-YFP is shown in blue, the fitter strain yNK-RFP is shown in yellow. The initial portion of yNK-RFP in this case was 4.5 %.

### 3.4. Establishment rates for different species and different growth temperatures

Strain pair	Temperature	Number of colonies
NEB	37°C	129
NEB neutral	37°C	58
NEB	30°C	108
NEB	RT	105
REL	37°C	79
REL	30°C	15
SJNEB	37°C	10
Yeast	30°C	15
Yeast neutral	30°C	150
JE41	37°C	5
JE44	37°C	10

Table 3.1.: Number of colonies analyzed for determining establishment rates.

Figure 3.12 shows the measured establishment rates of all strains we investigated plotted against the respective fitness advantages of the fitter strain with double-logarithmic scale. Since the datapoints for the neutral strain pairs cannot be seen completely in this graph, we show the data again with linear scale in Figures 3.13 and 3.14. Horizontal errorbars show deviation of  $\pm 10^\circ$  in measuring the asymptotic angle of a sector for determining the fitness advantage (see section 2.9). Vertical errorbars denote the error  $\sigma_{\langle E \rangle}$  calculated according to sections 2.8 and appendix D.

Table 3.1 shows the number of colonies that were analyzed for determining establishment rates.

The establishment rates cover a very large range starting at 20 reaching to about 10,000. Our results show clearly that establishment rates of high-noise systems (rod-like *E. coli* at 37°C and 30°C) are distinctly smaller than establishment rates of low-noise systems (*S. cerevisiae*, spherical *E. coli*, rod-like *E. coli* at room temperature). In the graphs we put a horizontal line at  $E = 450$  (cyan) to illustrate the separation of low- and high-noise systems.

Since fitness differences in most of the pairs are comparable (between 2 and 10 %), the fitness differences cannot explain the wide range of establishment rates. All the more, as the establishment rate should only grow with the square-root of  $s$  [4] (see equation 1.14).

### 3. Results

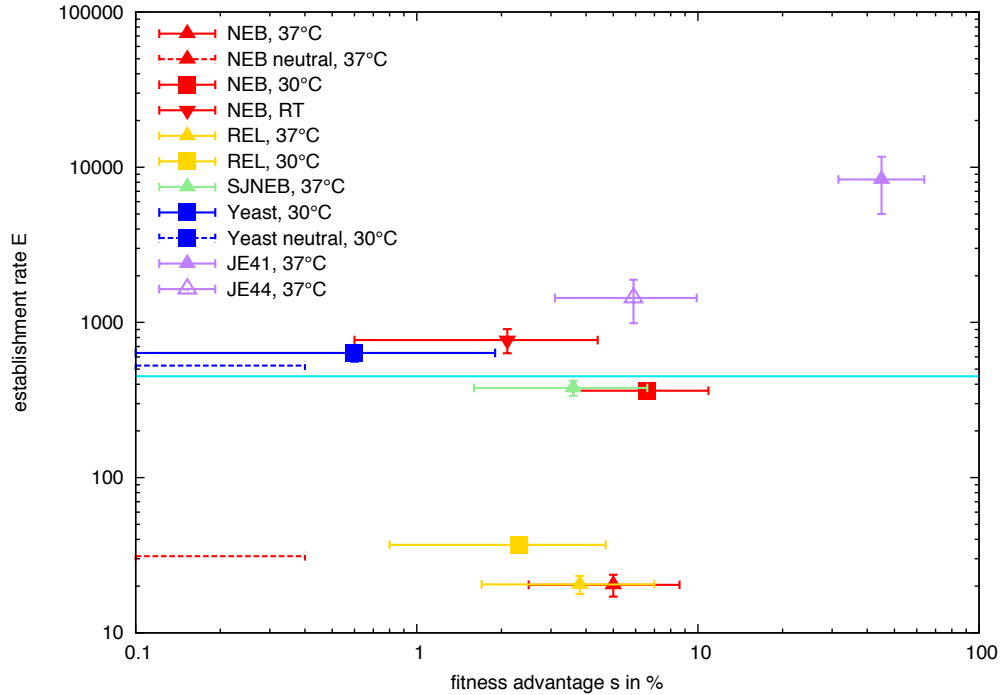


FIGURE 3.12.: **The establishment rate  $E$  versus the selective advantage of the mutant  $s$  (double-logarithmic scale).** Each data point shows the weighted average of  $E$  from a number of experiments with the same strains and the same temperature. Horizontal errorbars show deviation of  $\pm 10^\circ$  in measuring the asymptotic angle of a sector for determining the fitness advantage (see section 2.9 for details). Vertical errorbars denote the corrected error for the weighted average  $\sigma_{\langle E \rangle}$  (see sections 2.8.2 and appendix D). We observe a clear separation (cyan line) between high-noise systems (NEB, 37°C; NEB neutral, 37°C; NEB, 30°C; REL, 37°C; REL, 30°C; SJNEB, 37°C;) and low-noise systems (NEB, RT; Yeast, 30°C; Yeast, 30°C; Yeast neutral, 30°C; JE41, 37°C; JE44, 37°C).

### 3.4. Establishment rates for different species and different growth temperatures

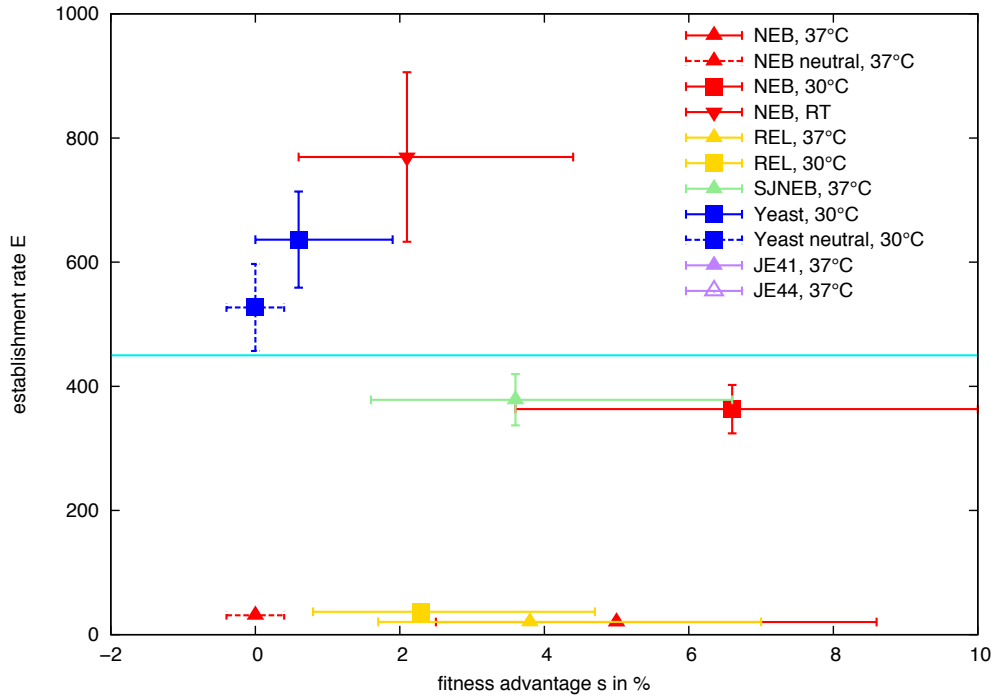


FIGURE 3.13.: **The establishment rate  $E$  versus the selective advantage of the mutant  $s$  (linear scale, w/o large establishment rates).** Each data point shows the weighted average of  $E$  from a number of experiments with the same strains and the same temperature. Horizontal errorbars show deviation of  $\pm 10^\circ$  in measuring the asymptotic angle of a sector for determining the fitness advantage (see section 2.9 for details). Vertical errorbars denote the corrected error for the weighted average  $\sigma_{\langle E \rangle}$  (see sections 2.8.2 and appendix D).

### 3. Results

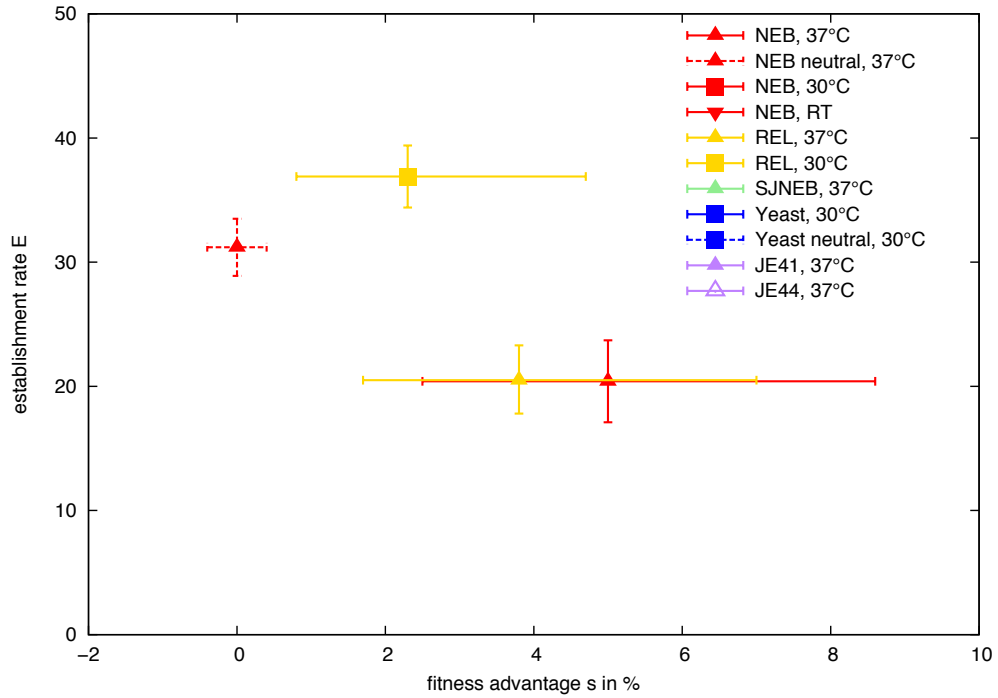


FIGURE 3.14.: **The establishment rate  $E$  versus the selective advantage of the mutant  $s$  (linear scale, only small establishment rates).** Each data point shows the weighted average of  $E$  from a number of experiments with the same strains and the same temperature. Horizontal errorbars show deviation of  $\pm 10^\circ$  in measuring the asymptotic angle of a sector for determining the fitness advantage (see section 2.9 for details). Vertical errorbars denote the corrected error for the weighted average  $\sigma_{\langle E \rangle}$  (see sections 2.8.2 and appendix D).

## 3.5. Control: Influence of inoculation volume

Since the inoculation volume varies between experiments, we tested the impact of inoculation volume on the number of established sectors. We inoculated 39 colonies of *E. coli* strain pair NEB at the same ratio and measured the inoculum size. After colonies had grown we counted the number of established sectors.

Figure 3.15 shows the number of established sectors of NEB-CFP mut as a function of the inoculum size. One can see that the data points are rather scattered and do not show an obvious trend. Nevertheless, we fitted the data via linear regression. The resulting slope is  $0.82 \pm 0.31 \text{ mm}^{-1}$ . The correlation coefficient between sector number and inoculation diameter is 0.40. From this data we assume that variation in inoculum sizes within our experiments does not explain the clear and large measured differences in establishment rates.

### 3. Results

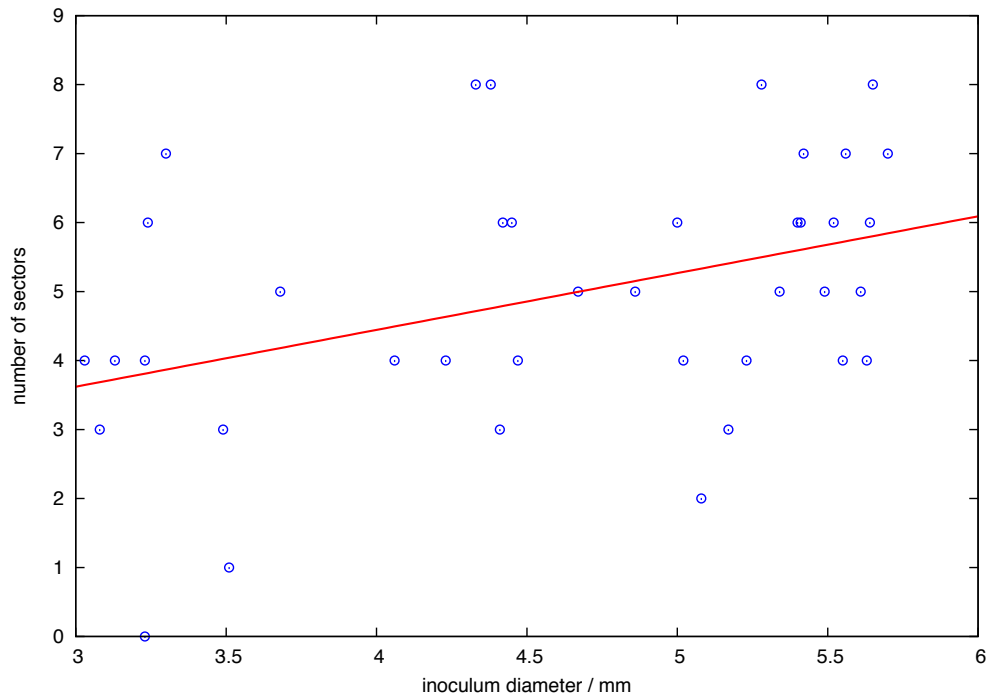


FIGURE 3.15.: **Control: Established sectors versus diameter of inoculum.**

Data were fitted via linear regression. The slope of the fitted line is  $0.82 \pm 0.31$   $\text{mm}^{-1}$ . The correlation coefficient between sector number and inoculation diameter is 0.40.

## 3.6. Control: Influence of total cell concentration

In our colonies we only measured the portion of mutant cells within the liquid culture. The total cell concentration was not determined and might have varied. The variation, however, should not have differed by an order of magnitude, since we always used overnight cultures grown to saturation.

To test, if a variation of total cell concentration has an effect on the number of establishment events, we conducted another control experiment. We inoculated colonies with undiluted mixture of overnight cultures, as well as with the same mixture, but diluted 10-fold, 100-fold (*E. coli* and *S. cerevisiae*) and 1000-fold (only *E. coli*). We then counted the resulting established sectors and calculated the establishment rate  $E$ . Figure 3.16 shows the results for *E. coli* and *S. cerevisiae*. For *E. coli*, 10-fold and 100-fold dilution has no effect on the establishment rate. At 1000-fold dilution, the establishment rate is slightly reduced. In the case of *S. cerevisiae*, the establishment rate hardly drops at 10-fold dilution, but is only at 100-fold dilution distinctly smaller.

Since dilution up to 10-fold hardly has an impact on the measured establishment rate, we conclude that possible variations of total cell concentration do not affect the results of our study.

### 3. Results

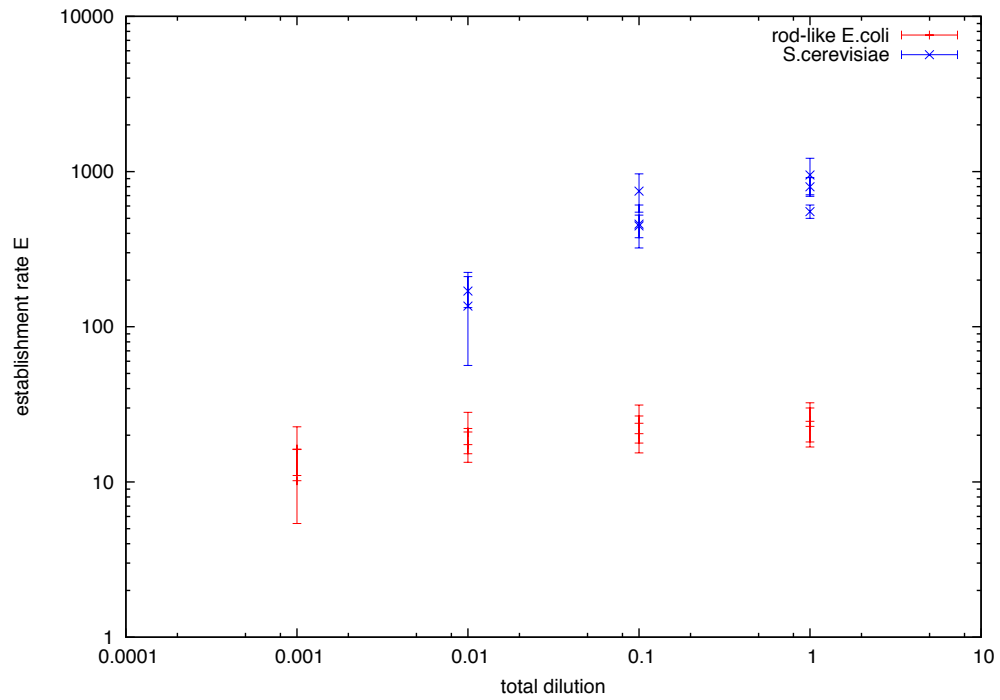


FIGURE 3.16.: **The establishment rate  $E$  versus the total dilution.** (Total dilution of e.g. 0.1 means that the total cell concentration of the inoculum was 0.1 times the concentration of the mixture of liquid overnight cultures.) Vertical errorbars denote the corrected error for the weighted average  $\sigma_{\langle E \rangle}$  (see sections 2.8.2 and appendix D).

## 4. Discussion

In this study we investigated the establishment of beneficial mutations during range expansions in spatially structured microbial populations. We presented a method for measuring establishment rates and found that these rates strongly vary between different species and growth conditions. In this chapter we summarize and interpret our findings.

### 4.1. Rod-like cell shape promotes high noise

Existing studies have stated that the type of sectors in microbial colonies is a measure of genetic drift [3] [4]. Straight sector boundaries lead to a large number of sectors corresponding to little loss of genetic diversity. In contrast, ragged sector boundaries cause more lineages to go extinct and therefore the colony ends up with less sectors. Colonies of ellipsoidal budding yeast *S. cerevisiae* exhibit many straight sectors, whereas rod-shaped bacteria *E. coli* and *P. aeruginosa* produce few ragged sectors.

Here we have shown that spherical mutants of *E. coli* produce colonies with straight sector boundaries like in the case of *S. cerevisiae*. Therefore, cell shape is one of the factors determining the type of sectors in colonies. However, it is not the only factor. We showed that colonies of rod-like fission yeast exhibit straight sectors as well. Thus, rod-like cell shape is not sufficient for causing high genetic drift, however, it might be necessary.

From our microscope images of rod-like *E. coli* we see that the typical distance between two kinks in a sector boundary is several tens of micrometers. This is probably due to aligning of the rod-like cells [55]. A correlation across several tens of micrometers means alignment across tens of cell diameters. We therefore presume that cell-to-cell adhesion and pressure are other crucial parameters in determining the level of noise in growing microbial colonies.

## 4.2. Growth temperature influences noise level

We have demonstrated that lower growth temperatures lead to less noise in colonies of *E. coli*. The reasons for this behavior remain unknown, yet. However, the different growth rates and corresponding expanding velocities might be the key to that question.

We have measured growth rates of *E. coli* and *S. cerevisiae* both in liquid culture and in colonies. Our results approve that in liquid as well as on plates at room temperature growth rates are drastically reduced compared to the usual growth temperatures of 37°C and 30°C.

Computer simulations like the ones in [56] may be a promising method to study the connection between growth rate and noise level.

## 4.3. Number of establishment events is proportional to mutant portion

Throughout the rest of our study we took the different noise levels in microbial colonies as a phenomenological parameter. We investigated the consequences of the different noise levels on the establishment of beneficial mutations. In order to do so, we mixed liquid culture of microbes with small portions of fitter mutants, grew colonies from the mixture and counted the resulting sectors established by the mutant.

We have shown that for sufficiently small mutant portions, the number of established sectors is proportional to the mutant portion. That allowed us to define the establishment rate as the ratio of sector number and mutant portion. This way the establishment rate is independent of the mutant portion.

## 4.4. Establishment rates range over three orders of magnitude

We have measured establishment rates for several strains of *E. coli* and *S. cerevisiae*. We have shown that establishment rates of low-noise systems (*S. cerevisiae*, spherical *E. coli* and rod-like *E. coli* grown at room temperature) are in the interval between 450 and 10,000. In contrast, establishment rates of high-noise systems (rod-like *E. coli* grown at 30°C and 37°C) range from 20 to 450. Thus, the efficiency of

#### 4.5. Variations of inoculation volume

natural selection in growing biofilms depends strongly on the species and growth conditions.

We have shown that the very same strains of *E. coli* exhibit largely different establishment rates at different growth temperatures. Therefore we can conclude that phylogenetic differences cannot explain the wide range of establishment rates. Instead, the same species can exhibit drastically different establishment rates depending on the growth conditions, in particular temperature.

This should be taken into account in future studies on adaptation in spatially structured populations.

### 4.5. Variations of inoculation volume do not explain the large differences between establishment rates in our experiments

We have shown that within the range of inoculation volumes in our experiments the establishment rate and the volume are only weakly correlated. Therefore we can exclude artifacts in our results caused by variations of inoculation volumes.

### 4.6. Establishment rate is independent of total cell concentration under crowded conditions

We have shown that the establishment rate is not affected by reduction of total cell concentration by at least a factor of 10 in *S. cerevisiae*. In the case of *E. coli*, even dilution of saturated liquid culture by a factor of 1000 does not change the establishment rate by more than a factor of 3. Thus, under crowded conditions establishment rate only very weakly depends on total cell concentration.

The different behavior of the two species is not a surprise, since their liquid culture saturation concentrations are different. Saturation concentration of *S. cerevisiae* in YPD is on the order of  $10^6$  cells / mL. In contrast, *E. coli* in LB reach saturation concentrations on the order of  $10^9$  cells / mL (Figure 3.5).

Knowing that under crowded conditions *E* rate does not depend on the total number of cells at the front,  $N_{front}$ , tells us something about the establishment probability. From equation 1.13 we can conclude that  $P_{est}$  is inversely proportional to  $N_{front}$  under crowded conditions. This is also what one would expect, since all cells at the front compete for expansion. The less competitors, the higher is the chance of a particular individual to succeed in colonizing the new territory.

## 4.7. Conclusion

In this study we have shown that the efficiency of natural selection in growing biofilms strongly depends on the species and the growth conditions. This is in contrast to the situation in well-mixed microbial populations. Assuming that mutation rates in the different systems studied are comparable, our results suggest that the speed of adaptation is strongly dependent on species and growth conditions in biofilms. In this case our results suggest that *E. coli* have a much lower adaptability in biofilms than *S. cerevisiae*.

One might speculate about an evolutionary advantage of low adaptability within biofilms. A species that changes between well-mixed conditions and biofilms frequently, might decrease its overall fitness when accumulating biofilm-specific advantages quickly. After all, these advantages could turn out deleterious during well-mixed growth.

In conclusion, our findings show an important phenomenon in growing biofilms that is not present in well-mixed microbial populations.

## 5. Outlook

The method to determine establishment rates presented in this study is simple and can be applied in the future to a variety of systems. Different species, growth temperatures and more parameters like nutrient and agar concentration can be tested. This is of particular interest, because of the great variety of shapes, microbial colonies exhibit depending on nutrient concentration, humidity and hardness of the agar plates [40] [57]. The next step might be measuring establishment rates of *S. pombe* and *P. aeruginosa*.

Instead of already having a fitter mutant in the inoculum, one could utilize spontaneous mutations of known rate. Plasmid loss is a good candidate here. A plasmid conferring resistance to an antibiotic and containing a fluorescence marker (like the ones used in our study) is deleterious, if the growth medium does not contain antibiotic. This is because expression of the marker gene costs resources. Plasmid loss can be easily detected in this case because of the loss of fluorescence. Thus, plasmid loss rates can be determined for instance via fluorescence activated cell sorting (FACS). In colony assays, cells that have lost the plasmid, form non-fluorescent sectors that can be counted, allowing for the exact experimental procedure as presented in this study.

Aside from that, the measurement of fitness differences can be improved. More precise methods are presented in [45].

The other still open key question is about what causes the differences in noise-level between different systems. The first step in addressing this question may be monitoring the growth of colonies on the single-cell level. Another approach are computer simulations similar to the ones in [56] that can implement different cell shapes and cell-to-cell adhesion strengths.

## 5. Outlook

# A. Biochemical protocols

The protocols for competent *E. coli* and heat-shock transformation are based on [58].

## A.1. Competent *E. coli*

### A.1.1. Composition of transfer buffer 1 (TFB1)

100 mM	RbCl
10 mM	CaCl <sub>2</sub>
50 mM	MnCl <sub>2</sub>
30 mM	Potassium acetate
15 %	Glycerol

Adjust to pH 5.8 by adding HCl. Sterile-filter and store at 4°C.

### A.1.2. Composition of transfer buffer 2 (TFB2)

10 mM	RbCl
75 mM	CaCl <sub>2</sub>
10 mM	MOPS
15 %	Glycerol

Adjust to pH 6.8 by adding KOH. Sterile-filter and store at 4°C.

## A. Biochemical protocols

### A.1.3. Procedure

1. Grow *E. coli* overnight in LB.
2. Add 333  $\mu\text{L}$  of overnight culture to 33 mL pre-warmed LB in a sterile Erlenmeyer flask and grow to an OD of 0.5.
3. Cool on ice for 5 min.
4. Centrifuge at 4°C and 4000 g for 5 min. Remove supernatant.
5. Resuspend pellet in 10 mL ice-cold TFB1.
6. Store on ice for 90 min.
7. Centrifuge at 4°C and 4000 g for 5 min. Remove supernatant.
8. Resuspend pellet in 666  $\mu\text{L}$  ice-cold TFB2.
9. Aliquot to 100–200  $\mu\text{L}$ .
10. Flash-freeze in liquid nitrogen.
11. Store at -80°C.

## A.2. Transformation of *E. coli*

### A.2.1. Procedure

1. Thaw competent cells on ice.
2. Add 1  $\mu\text{L}$  of plasmid DNA eluate.
3. Store on ice for 20 min.
4. Heat-shock at 42°C in water bath for 90 s.
5. Add 1 mL LB.
6. Shake at 400 rpm at 37°C for 60 min.
7. Plate 50 – 200  $\mu\text{L}$  on LB agar containing 0.1 g/L ampicillin.

## B. Microscopy

In section 2.3 we described our microscope setup and in section 2.7 we explained the method to determine initial mutant portions. Here we show images of the microscope and the cell counting device.

*B. Microscopy*

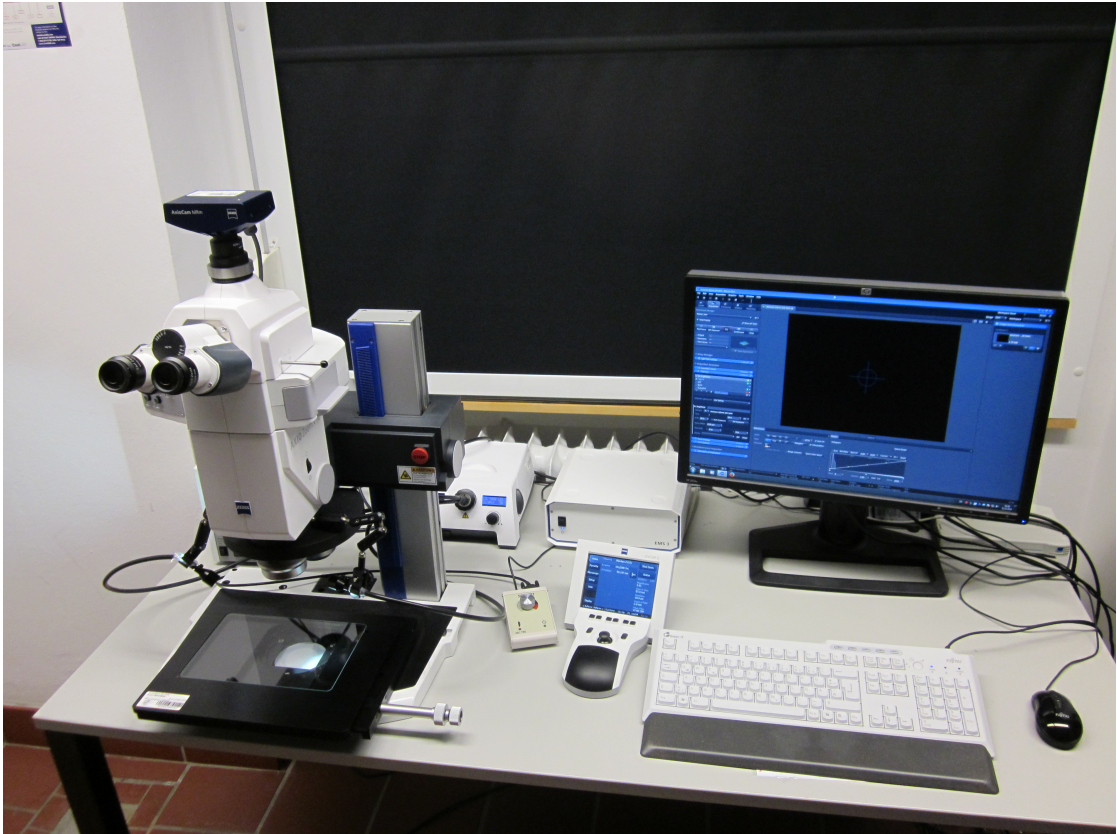
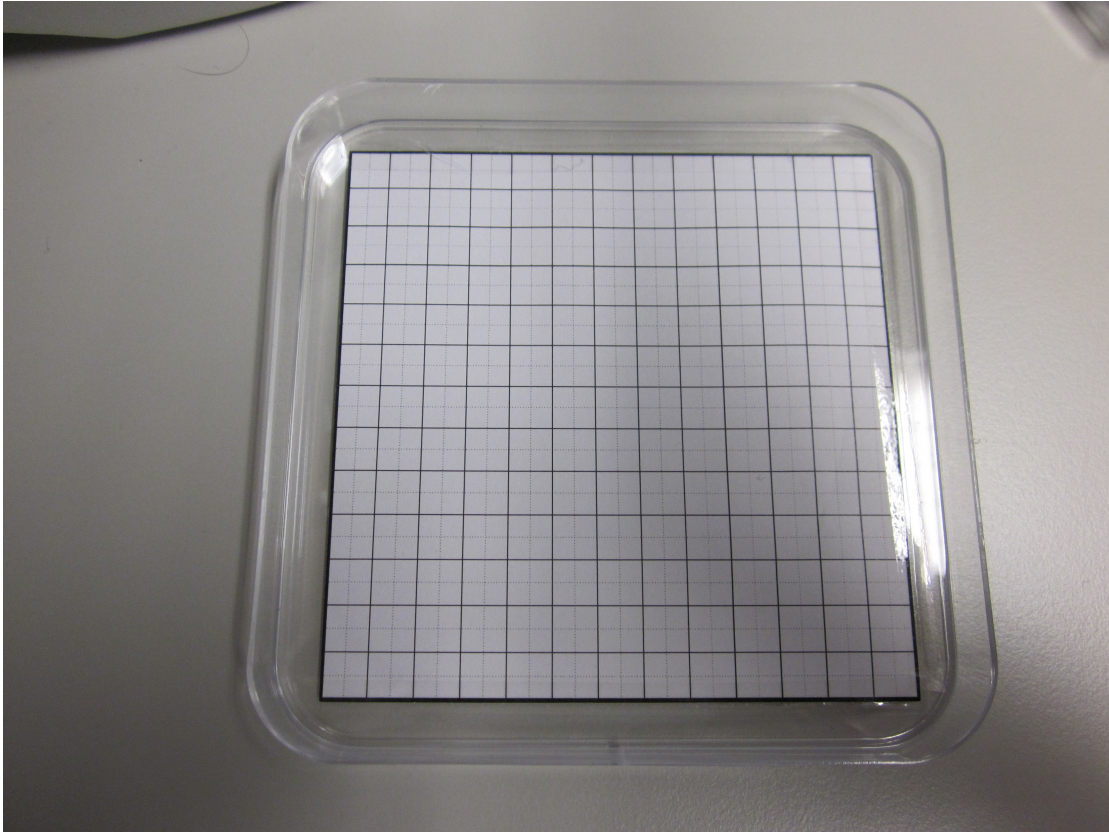
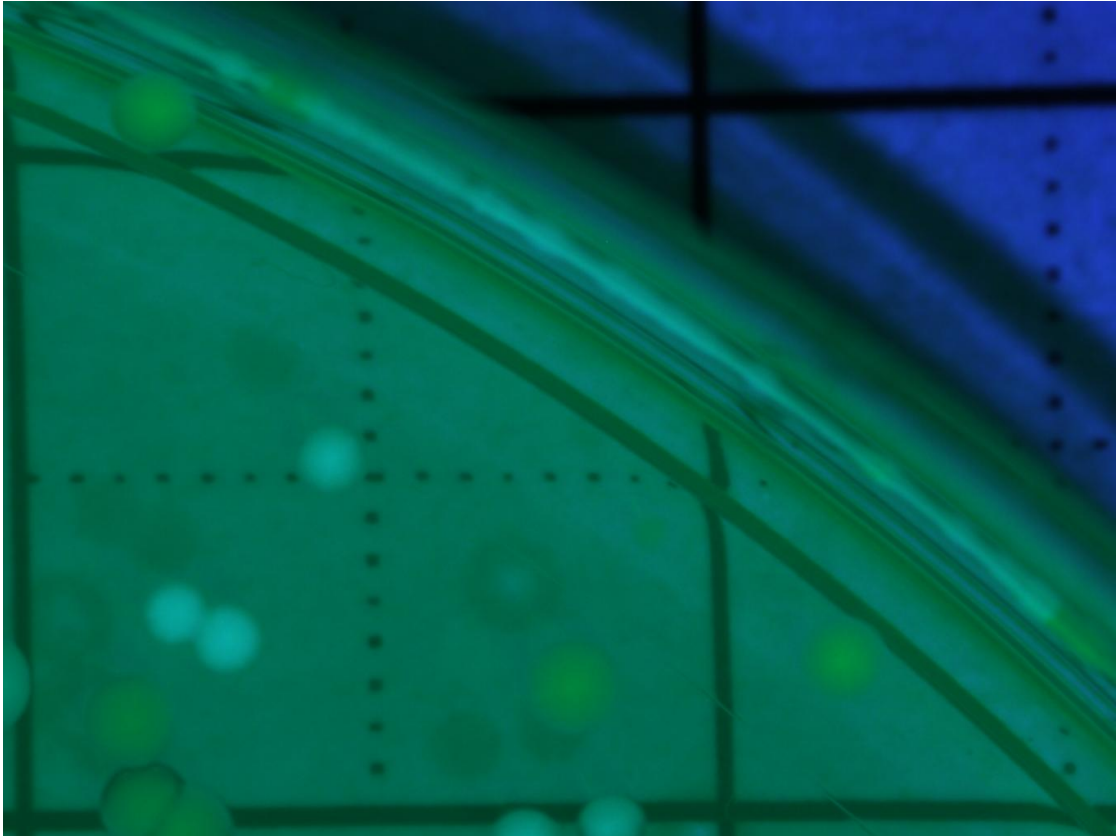


FIGURE B.1.: **Stereomicroscope.** Zeiss AxioZoom.V16 microscope with LED illumination (CL 9000 LED) for brightfield imaging, a metal-halide lamp (HXP 200 C) for fluorescence imaging and an AxioCam MRm camera.



**FIGURE B.2.: Device used for counting colonies.** A sheet of paper with a printed grid on it was stuck onto a quadratic petri dish. To count fluorescent colonies on an agar plate, the respective plate was put onto the grid and both were placed under the fluorescent microscope.

*B. Microscopy*



**FIGURE B.3.:** Microscope image: edge of an agar plate with colonies of two different fluorescent colors (green and cyan). The fluorescent colors are clearly distinguishable. You can see the grid of the counting device below the agar plate.

## C. Colonies

In section 3.4 we showed microscope images of one REL and one Yeast colony with established sectors of the fitter strain of the pair. Here we show respective images of one colony of NEB (Figure C.1) and one of JE44 (Figure C.3).

*C. Colonies*

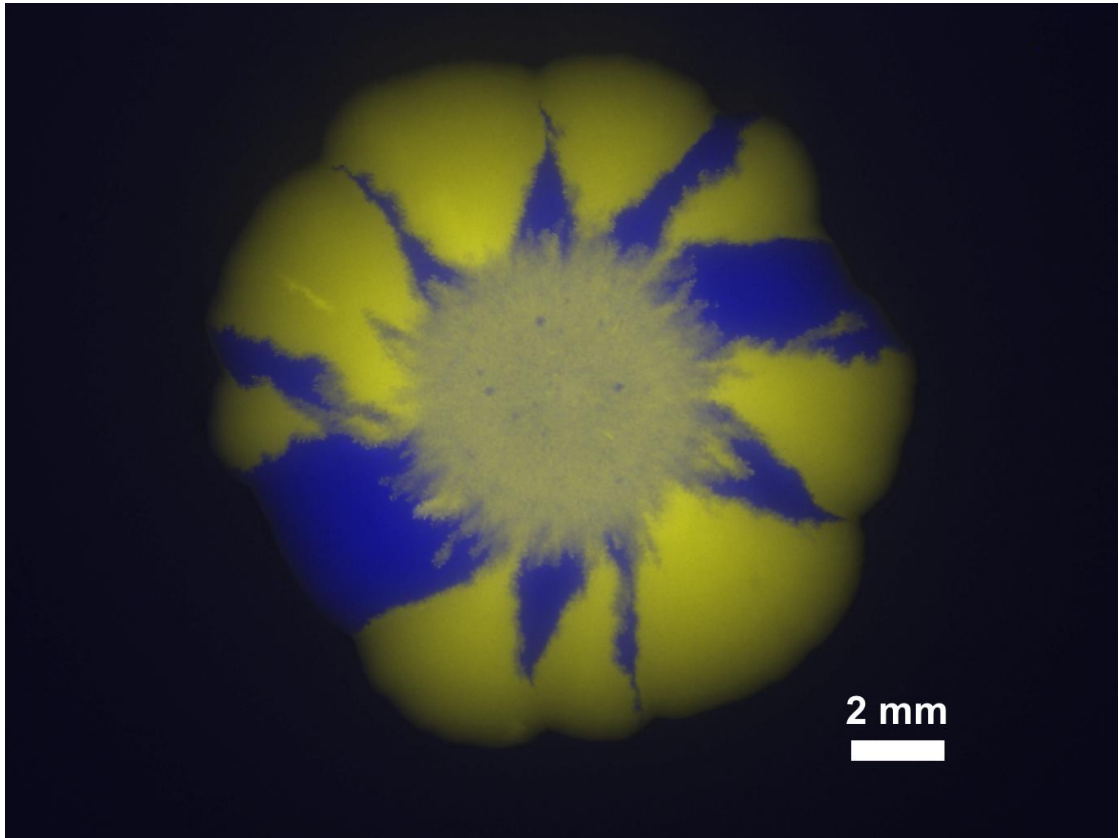


FIGURE C.1.: **Established sectors of rod-like *E. coli* strain pair NEB.** NEB-YFP is shown in blue, the fitter strain NEB-CFP mut is shown in yellow. The initial portion of NEB-CFP mut in this case was 33 %.

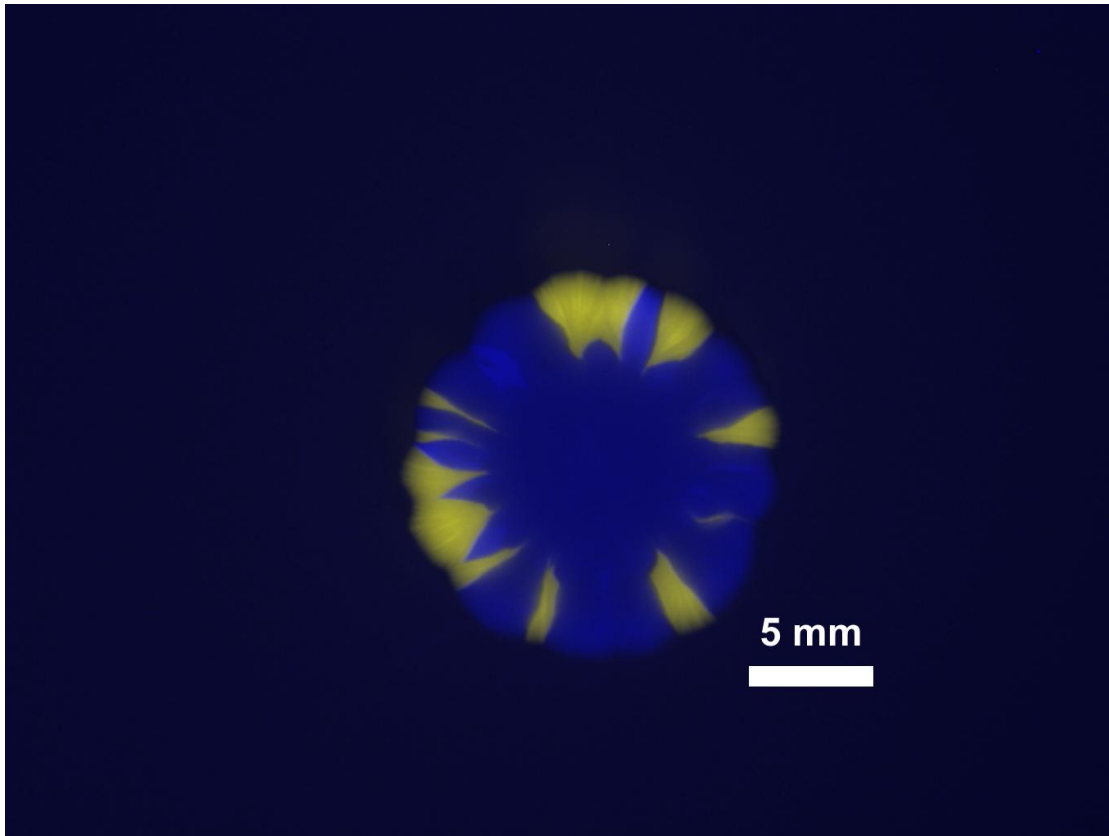


FIGURE C.2.: Established sectors of spherical *E. coli*.

FIGURE C.3.: Established sectors of spherical *E. coli* strain pair JE44. JE-CFP4 is shown in blue, the fitter strain JE-YFP4 mut is shown in yellow. The initial portion of JE-YFP4 mut in this case was 0.90 %.

*C. Colonies*

## D. Estimation of errors in establishment rate

For each experiment and each mutant portion  $p_{mut}$  we calculated the arithmetic mean of the sector numbers in our replicates and the corresponding standard error  $\sigma_{sec}$ . The error of  $p_{mut}$  was determined as follows: The number of mutant colonies on our counting plates should follow a binomial distribution:

$$P_m(k) = \binom{m}{k} (1 - p_{mut})^{m-k} p_{mut}^k . \quad (D.1)$$

Here  $P_m(k)$  is the probability that in a sample of  $m$  cells we find  $k$  mutant cells, given that the portion of mutant cells in the total population is  $p_{mut}$ .

One can calculate the Clopper-Pearson confidence interval [59] using quantiles of the Beta distribution [60]:

$$B\left(\frac{\alpha}{2}, k, m - k + 1\right) = p_{lb} < p_{mut} < p_{ub} = B\left(1 - \frac{\alpha}{2}, k + 1, m - k\right) , \quad (D.2)$$

where  $\alpha$  is the error percentile,  $B$  is the inverse of the Beta cumulative distribution function and  $p_{lb}$  and  $p_{ub}$  are the lower and the upper bound of the confidence interval. We choose to calculate the 95% confidence interval, therefore  $\alpha = 5\%$ .

Since  $n_{sec} \in [n_{sec} - \sigma_{sec}; n_{sec} + \sigma_{sec}]$  at 68% probability we can conclude

$$\frac{(n_{sec} - \sigma_{sec})}{p_{ub}} =: E_{lb} < E < E_{ub} := \frac{(n_{sec} + \sigma_{sec})}{p_{lb}} \quad (D.3)$$

at  $\approx 65\%$ .

We take the maximum of  $E_{ub} - E$  and  $E - E_{lb}$  and define it as the deviation  $\sigma_E$ . This way we get errorbars for one set of experiments at one specific mutant portion.

In order to obtain one single data point for each set of experiments with equal strains and temperature we calculate the weighted average of  $E$  over all mutant portions:

D. Estimation of errors in establishment rate

$$\langle E \rangle = \frac{\sum_i \frac{E_i}{\sigma_{E_i}^2}}{\sum_i \frac{1}{\sigma_{E_i}^2}}. \quad (\text{D.4})$$

Since for a given set of experiments the  $\sigma_{E_i}$  may vary quite strongly, the estimation of the resulting error of the weighted average via

$$\tilde{\sigma}_{\langle E \rangle} = \sqrt{\frac{1}{\sum_i \frac{1}{\sigma_{E_i}^2}}} \quad (\text{D.5})$$

might not be precise enough, and the corrected error

$$\hat{\sigma}_{\langle E \rangle} = \sqrt{\frac{\sum_i \frac{(E_i - \langle E \rangle)^2}{\sigma_{E_i}^2}}{(N - 1) \sum_i \frac{1}{\sigma_{E_i}^2}}} \quad (\text{D.6})$$

is a better estimate,  $N$  being the number of experiments in the set. In our graphs we always show the greater of the two errors:

$$\sigma_{\langle E \rangle} = \max \left( \sqrt{\frac{1}{\sum_i \frac{1}{\sigma_{E_i}^2}}}, \sqrt{\frac{\sum_i \frac{(E_i - \langle E \rangle)^2}{\sigma_{E_i}^2}}{(N - 1) \sum_i \frac{1}{\sigma_{E_i}^2}}} \right). \quad (\text{D.7})$$

## Acknowledgements

First of all, I want to thank my supervisor Oskar Hallatschek, who gave me the opportunity to work in his lab. I enjoyed the time in the evolutionary dynamics group, and my knowledge of science underwent quite a range expansion, while I accumulated many beneficial insights. Oskar never ran out of ideas when experimental challenges had to be taken. Moreover, when I struggled with a number of personal problems during my PhD time, he supported me very well and helped me to get back on track.

I'd also like to thank my co-supervisors Christoph F. Schmidt and Daniel Jackson for fruitful discussions and helpful advice.

I want to thank all members of the evolutionary dynamics group: Erik A. Martens, Jens Nullmeier, Sven Boekhoff, Clemens Buss, Lukas Geyrhofer, Jörn Hartung, Jean-François Flot, Hedvika Toncova, Paulo Pinto, Christopher Seedig, Marc Szabo, Niels Podewitz, Matthias Meschede, Robert Filter, Martin Ehrle, Marijn Korsten, Jan Lebert, Diana Struever and Sabine Limmer. I had a great time with you!

A special thanks goes to Barbara Kutz who gave me a lot of practical as well as emotional support when I needed it the most.

Finally I want to thank my family and my friends. This work would not have been possible without them.

*D. Estimation of errors in establishment rate*

# Bibliography

- [1] J William Costerton, KJ Cheng, Gill G Geesey, Timothy I Ladd, J Curtis Nickel, Mrinal Dasgupta, and Thomas J Marrie. Bacterial biofilms in nature and disease. *Annual Reviews in Microbiology*, 41(1):435–464, 1987.
- [2] Daniel López, Hera Vlamakis, and Roberto Kolter. Biofilms. *Cold Spring Harbor perspectives in biology*, 2(7):a000398, 2010.
- [3] Oskar Hallatschek, Pascal Hersen, Sharad Ramanathan, and David R Nelson. Genetic drift at expanding frontiers promotes gene segregation. *Proceedings of the National Academy of Sciences*, 104(50):19926–19930, 2007.
- [4] Oskar Hallatschek and David R Nelson. Life at the front of an expanding population. *Evolution*, 64(1):193–206, 2010.
- [5] David Wacey, Matt R Kilburn, Martin Saunders, John Cliff, and Martin D Brasier. Microfossils of sulphur-metabolizing cells in 3.4-billion-year-old rocks of western australia. *Nature Geoscience*, 4(10):698–702, 2011.
- [6] Yoko Ohtomo, Takeshi Kakegawa, Akizumi Ishida, Toshiro Nagase, and Minik T Rosing. Evidence for biogenic graphite in early archaean isua metasedimentary rocks. *Nature Geoscience*, 7(1):25–28, 2014.
- [7] Carl Von Linne. *Systema naturae per regna tria naturae secundum classes, ordines, genera, species cum characteribus, differentiis, synonymis, locis; editio duodecima.*, volume 1. Salvius, 1766.
- [8] Godfrey Hewitt. The genetic legacy of the quaternary ice ages. *Nature*, 405(6789):907–913, 2000.
- [9] I-Ching Chen, Jane K Hill, Ralf Ohlemüller, David B Roy, and Chris D Thomas. Rapid range shifts of species associated with high levels of climate warming. *Science*, 333(6045):1024–1026, 2011.
- [10] Mark A Davis, Matthew K Chew, Richard J Hobbs, Ariel E Lugo, John J Ewel, Geerat J Vermeij, James H Brown, Michael L Rosenzweig, Mark R Gardener, Scott P Carroll, et al. Don’t judge species on their origins. *Nature*, 474(7350):153–154, 2011.

## Bibliography

- [11] Mark Stoneking and Johannes Krause. Learning about human population history from ancient and modern genomes. *Nature Reviews Genetics*, 12(9):603–614, 2011.
- [12] Stephen Oppenheimer. Out-of-africa, the peopling of continents and islands: tracing uniparental gene trees across the map. *Philosophical Transactions of the Royal Society B: Biological Sciences*, 367(1590):770–784, 2012.
- [13] Laurent Excoffier, Matthieu Foll, and Rémy J Petit. Genetic consequences of range expansions. *Annual Review of Ecology, Evolution, and Systematics*, 40:481–501, 2009.
- [14] Santiago F Elena and Richard E Lenski. Evolution experiments with microorganisms: the dynamics and genetic bases of adaptation. *Nature Reviews Genetics*, 4(6):457–469, 2003.
- [15] John H Gillespie. *Population genetics: a concise guide*. Johns Hopkins University Press, second edition, 2004.
- [16] Richard E Lenski. The e. coli long-term experimental evolution project site. <http://myxo.css.msu.edu/ecoli>, 2014.
- [17] Tracy L Ferea, David Botstein, Patrick O Brown, and R Frank Rosenzweig. Systematic changes in gene expression patterns following adaptive evolution in yeast. *Proceedings of the National Academy of Sciences*, 96(17):9721–9726, 1999.
- [18] Mlawule R Mashego, Mickel LA Jansen, Jacobus L Vinke, Walter M Gulik, and Joseph J Heijnen. Changes in the metabolome of *saccharomyces cerevisiae* associated with evolution in aerobic glucose-limited chemostats. *FEMS yeast research*, 5(4-5):419–430, 2005.
- [19] David Gresham, Michael M Desai, Cheryl M Tucker, Harry T Jenq, Dave A Pai, Alexandra Ward, Christopher G DeSevo, David Botstein, and Maitreya J Dunham. The repertoire and dynamics of evolutionary adaptations to controlled nutrient-limited environments in yeast. *PLoS genetics*, 4(12):e1000303, 2008.
- [20] Isabel Gordo and Paulo RA Campos. Adaptive evolution in a spatially structured asexual population. *Genetica*, 127(1-3):217–229, 2006.
- [21] Michelle GJL Habets, Tamas Czarán, Rolf F Hoekstra, and J Arjan GM de Visser. Spatial structure inhibits the rate of invasion of beneficial mutations in asexual populations. *Proceedings of the Royal Society B: Biological Sciences*, 274(1622):2139–2143, 2007.

- [22] Paulo RA Campos, Pedro SCA Neto, Viviane M De Oliveira, and Isabel Gordo. Environmental heterogeneity enhances clonal interference. *Evolution*, 62(6):1390–1399, 2008.
- [23] Erik A Martens and Oskar Hallatschek. Interfering waves of adaptation promote spatial mixing. *Genetics*, 189(3):1045–1060, 2011.
- [24] Bronwyn E Ramey, Maria Koutsoudis, Susanne B von Bodman, and Clay Fuqua. Biofilm formation in plant–microbe associations. *Current opinion in microbiology*, 7(6):602–609, 2004.
- [25] Mark W LeChevallier, Timothy M Babcock, and Ramon G Lee. Examination and characterization of distribution system biofilms. *Applied and Environmental Microbiology*, 53(12):2714–2724, 1987.
- [26] Vincent Zijngel, M Barbara M van Leeuwen, John E Degener, Frank Abbas, Thomas Thurnheer, Rudolf Gmür, and Hermie JM Harmsen. Oral biofilm architecture on natural teeth. *PloS one*, 5(2):e9321, 2010.
- [27] GG Anderson and GA O’toole. Innate and induced resistance mechanisms of bacterial biofilms. In *Bacterial biofilms*, pages 85–105. Springer, 2008.
- [28] Mark A Schembri, Kristian Kjærgaard, and Per Klemm. Global gene expression in escherichia coli biofilms. *Molecular microbiology*, 48(1):253–267, 2003.
- [29] Steven S Branda, José Eduardo González-Pastor, Sigal Ben-Yehuda, Richard Losick, and Roberto Kolter. Fruiting body formation by bacillus subtilis. *Proceedings of the National Academy of Sciences*, 98(20):11621–11626, 2001.
- [30] Marvin Whiteley, M Gita Bangera, Roger E Bumgarner, Matthew R Parsek, Gail M Teitzel, Stephen Lory, and EP Greenberg. Gene expression in pseudomonas aeruginosa biofilms. *Nature*, 413(6858):860–864, 2001.
- [31] Karin Sauer, Anne K Camper, Garth D Ehrlich, J William Costerton, and David G Davies. Pseudomonas aeruginosa displays multiple phenotypes during development as a biofilm. *Journal of bacteriology*, 184(4):1140–1154, 2002.
- [32] Karen E Beenken, Paul M Dunman, Fionnuala McAleese, Daphne Macapagal, Ellen Murphy, Steven J Projan, Jon S Blevins, and Mark S Smeltzer. Global gene expression in staphylococcus aureus biofilms. *Journal of bacteriology*, 186(14):4665–4684, 2004.
- [33] Zdena Palková. Multicellular microorganisms: laboratory versus nature. *EMBO reports*, 5(5):470–476, 2004.

## Bibliography

- [34] Kevin Laland, Tobias Uller, Marc Feldman, Kim Sterelny, Gerd B Müller, Armin Moczek, Eva Jablonka, John Odling-Smee, Gregory A Wray, Hopi E Hoekstra, et al. Does evolutionary theory need a rethink? *Nature*, 514(7521):161, 2014.
- [35] Joao B Xavier and Kevin R Foster. Cooperation and conflict in microbial biofilms. *Proceedings of the National Academy of Sciences*, 104(3):876–881, 2007.
- [36] John H Koschwanez, Kevin R Foster, and Andrew W Murray. Sucrose utilization in budding yeast as a model for the origin of undifferentiated multicellularity. *PLoS biology*, 9(8):e1001122, 2011.
- [37] Melanie JI Müller, Beverly I Neugeboren, David R Nelson, and Andrew W Murray. Genetic drift opposes mutualism during spatial population expansion. *Proceedings of the National Academy of Sciences*, 111(3):1037–1042, 2014.
- [38] Robert Axelrod and William D Hamilton. The evolution of cooperation. *Science*, 211(4489):1390–1396, 1981.
- [39] Martin A Nowak. Five rules for the evolution of cooperation. *science*, 314(5805):1560–1563, 2006.
- [40] M Matsushita, J Wakita, H Itoh, K Watanabe, T Arai, T Matsuyama, H Sakaguchi, and M Mimura. Formation of colony patterns by a bacterial cell population. *Physica A: Statistical Mechanics and its Applications*, 274(1):190–199, 1999.
- [41] Ronald Aylmer Fisher. The wave of advance of advantageous genes. *Annals of Eugenics*, 7(4):355–369, 1937.
- [42] AN Kolmogorov, IG Petrovskii, and NS Piskunov. A study of the equation of diffusion with increase in the quantity of matter, and its application to a biological problem. *Bjul. Moskovskogo Gos. Univ*, 1(7):1–26, 1937.
- [43] James D Murray. *Mathematical biology i: An introduction*, vol. 17 of interdisciplinary applied mathematics, 2002.
- [44] Oskar Hallatschek and David R Nelson. Population genetics and range expansions. *Phys. Today*, 62(7):42, 2009.
- [45] Kirill S Korolev, Melanie JI Müller, Nilay Karahan, Andrew W Murray, Oskar Hallatschek, and David R Nelson. Selective sweeps in growing microbial colonies. *Physical biology*, 9(2):026008, 2012.

- [46] Robert D Deegan, Olga Bakajin, Todd F Dupont, Greb Huber, Sidney R Nagel, and Thomas A Witten. Capillary flow as the cause of ring stains from dried liquid drops. *Nature*, 389(6653):827–829, 1997.
- [47] New England BioLabs Inc. Product website: Neb 5-alpha competent e. coli (high efficiency). <https://www.neb.com/products/c2987-neb-5-alpha-competent-e-coli-high-efficiency>.
- [48] Brian G Spratt. Distinct penicillin binding proteins involved in the division, elongation, and shape of escherichia coli k12. *Proceedings of the National Academy of Sciences*, 72(8):2999–3003, 1975.
- [49] William D Donachie, Stephen Addinall, and Ken Begg. Cell shape and chromosome partition in prokaryotes or, why e. coli is rod-shaped and haploid. *Bioessays*, 17(6):569–576, 1995.
- [50] Waldemar Vollmer and Joachim-Volker Höltje. Morphogenesis of escherichia coli. *Current opinion in microbiology*, 4(6):625–633, 2001.
- [51] Miguel A de Pedro, William D Donachie, Joachim-Volker Höltje, and Heinz Schwarz. Constitutive septal murein synthesis in escherichia coli with impaired activity of the morphogenetic proteins rodA and penicillin-binding protein 2. *Journal of bacteriology*, 183(14):4115–4126, 2001.
- [52] Felipe O Bendezú and Piet AJ de Boer. Conditional lethality, division defects, membrane involution, and endocytosis in mre and mrd shape mutants of escherichia coli. *Journal of bacteriology*, 190(5):1792–1811, 2008.
- [53] Denis Boyer, William Mather, Octavio Mondragón-Palomino, Sirio Orozco-Fuentes, Tal Danino, Jeff Hasty, and Lev S Tsimring. Buckling instability in ordered bacterial colonies. *Physical biology*, 8(2):026008, 2011.
- [54] Jacques Monod. The growth of bacterial cultures. *Annual Reviews in Microbiology*, 3(1):371–394, 1949.
- [55] Dmitri Volfson, Scott Cookson, Jeff Hasty, and Lev S Tsimring. Biomechanical ordering of dense cell populations. *Proceedings of the National Academy of Sciences*, 105(40):15346–15351, 2008.
- [56] FDC Farrell, O Hallatschek, D Marenduzzo, and B Waclaw. Mechanically driven growth of quasi-two-dimensional microbial colonies. *Physical review letters*, 111(16):168101, 2013.
- [57] Eshel Ben-Jacob, Inon Cohen, and Herbert Levine. Cooperative self-organization of microorganisms. *Advances in Physics*, 49(4):395–554, 2000.

*Bibliography*

- [58] Qiagen. *The QIAexpressionist*, fifth edition, 2003.
- [59] C. J. Clopper and E. S. Pearson. The use of confidence or fiducial limits illustrated in the case of the binomial. *Biometrika*, 26(4):pp. 404–413, 1934.
- [60] Lawrence D Brown, T Tony Cai, and Anirban DasGupta. Interval estimation for a binomial proportion. *Statistical Science*, pages 101–117, 2001.

# Curriculum Vitae

Name                   **Fabian Stiewe**  
born on                February, 1<sup>st</sup> 1985  
in                        Salzgitter

## Academic Education

2004 - 2010           **Physics**  
                          (Diploma)  
                          Georg-August-Universität Göttingen

2010 - 2014           **Physics**  
                          (PhD Candidate)  
                          Max Planck Institute for Dynamics and Self-Organization, and  
                          Georg-August-Universität Göttingen